AIMS Mathematics, 10(8): 19300–19334.
DOI: 10.3934/math.2025863
Received: 20 June 2025
Revised: 01 August 2025
Accepted: 13 August 2025
Published: 25 August 2025

https://www.aimspress.com/journal/Math

Research article

A light-tail Pareto Type II model for disability and reliability case studies with potential risk assessment under disability prevalence dates data in Saudi Arabia

Atef F. Hashem[1,2], Mohamed A. Abdelkawy[1] and Haitham M. Yousof[3,*]

[1] Department of Mathematics and Statistics, College of Science, Imam Mohammad Ibn Saud Islamic University (IMSIU), Riyadh 11432, Saudi Arabia
[2] King Salman Center for Disability Research, Riyadh 11614, Saudi Arabia
[3] Department of Statistics, Mathematics and Insurance, Benha University, Egypt

* **Correspondence:** Email: haitham.yousof@fcom.bu.edu.eg.

Abstract: We introduce a new flexible statistical model for disability and reliability case studies, designed to enhance modeling capabilities in reliability engineering and disability prevalence analysis. This model extends the classical Pareto Type II distribution by incorporating additional shape parameters, allowing for greater flexibility in modeling various hazard rate shapes and tail behaviors, particularly light tails. Essential properties of the model are explored. The model's applicability and risk assessment potential are demonstrated through case studies: one focusing on reliability engineering (aircraft windshield failure and service times) and another analyzing disability prevalence rates in Saudi Arabia for 2016. Advanced tail analysis tools such as the Hill estimator, Value-at-Risk (VaR), and Peaks Over a Random Threshold (PORT) were employed. The analyses reveal that the proposed OGPTII model offers superior goodness-of-fit compared to several existing models for both reliability and Saudi Arabia disability data, accurately captures the light-tailed nature of the datasets, and provides crucial insights into potential risk factors. This makes it a valuable tool for predictive maintenance strategies in engineering and for evidence-based policy planning and resource allocation in the context of disability management.

Keywords: disability prevalence data; Saudi Arabia disability data; risk assessment; reliability; aircraft windshield failure analysis; light-tail Pareto Type II model; tail index estimation; maximum likelihood estimation; extreme value analysis; statistical simulation; goodness-of-fit tests

Mathematics Subject Classification: 62N05, 62E11, 62H05, 62F10, 62P05, 62G32, 60E05, 62F15

1. Introduction

Analyzing disability prevalence data in the Kingdom of Saudi Arabia is not merely a statistical exercise, but a crucial step toward building a more inclusive and equitable society, especially within the framework of Saudi Vision 2030. This vision, which aims to diversify the economy and empower all segments of society, places strong emphasis on health, social welfare, and human potential, making the understanding of disability patterns essential for informed policymaking. With significant regional disparities in disability rates, ranging from just a few thousand cases in Al-Bahah to over 285,000 in the Northern Border region, a one-size-fits-all approach will not suffice. These variations point to deeper underlying factors such as access to healthcare, environmental conditions, demographic structures, and differences in reporting practices across regions. Accurate modeling of this data allows policymakers to allocate resources more effectively, design targeted intervention programs, and ensure that no community is left behind. In this paper, we introduce a new flexible statistical model, the Odd-Generalized Pareto Type II (OGPTII), specifically tailored to capture the complex nature of such real-world data. Unlike traditional models that may underestimate extreme values, the OGPTII excels in characterizing heavy-tailed behaviors, making it ideal for assessing the risk of high-concentration disability regions. Our analysis reveals that some areas face disproportionately high disability burdens, a reality that must be addressed to achieve social balance and economic fairness. By applying advanced risk assessment tools like VaR, Hill estimation, and PORT analysis, we provide a comprehensive view of potential future scenarios. The model's superior fit over existing distributions underscores its practical value in public health planning. Moreover, reliable estimation of tail risks ensures that emergency preparedness and long-term support systems are robust. This work supports the broader goals of Vision 2030 by promoting data-driven decision-making in social development. It highlights how statistical innovation can directly contribute to national priorities. Ultimately, understanding disability prevalence is about recognizing human dignity and ensuring equal opportunities. With better models come better policies, and with better policies comes a more just and resilient society.

Therefore, developing more flexible and robust statistical models has become essential for advancing reliability analysis and supporting informed decision-making. The Pareto Type II (PTII) distribution has long been recognized for its applicability in modeling extreme events and heavy-tailed phenomena. According to [1], it has been widely used in finance, insurance, and engineering due to its ability to represent rare but impactful occurrences. [2] further emphasized its importance in fitting firm size data, highlighting its relevance in economic modeling. The PTII model's flexibility makes it especially useful in risk assessment, where understanding tail behavior is crucial for predicting catastrophic failures or large financial losses.

Over the years, several extensions of the classical PTII distribution have been proposed to enhance modeling capabilities. Recently, [3] introduced a generalized version of the PTII model, offering improved statistical properties and broader applicability in real-life scenarios. Then, [4] developed a transmuted Weibull Pareto Type II model, which demonstrated superior performance in capturing different hazard rate shapes. [5] also contributed to this line of research by proposing another extension of the original PTII distribution, tailored for better fit across diverse datasets. [6]

validated a new version of the PTII model. Similarly, [7] explored a new version of the PTII model specifically designed for analyzing survival times and tax revenue data, reinforcing the model's versatility across domains. In recent years, the development of extended families of distributions has gained momentum in statistical literature. [8] introduced the generated odd exponential generalized (GOGE-G) family, which provides a general framework for generating more flexible models. This family allows for the derivation of new distributions capable of exhibiting increasing, decreasing, or bathtub-shaped hazard rates, features commonly observed in engineering systems subject to wear and aging.

Building upon these advancements, this paper introduces a new version of the PTII model called the OGPTII model. The OGPTII is derived from the GOGE-G family and offers enhanced adaptability in modeling both light and heavy-tailed data. It demonstrates promise in two real-life case studies involving aircraft windshield failure and service time data. These datasets are analyzed using advanced tools such as the Hill estimator, VaR, TVaR, and PORT analysis, which help quantify risk and assess tail behavior. The new model is derived from a new family derived based on the GOGE-G family, defined by [8]. The cumulative distribution function (CDF) of the GOGE-G family is presented as:

$$F_{\alpha,\beta}(x) = \left\{1 - exp\left[-\frac{G(x)^{\alpha}}{1-G(x)^{\alpha}}\right]\right\}^{\beta}, \tag{1}$$

where $G(x)$ is the base line model. Starting with (1), we define a new generalized CDF as follows:

$$F_{\alpha,\beta}(x) = (1 - \beta\, exp\{-[G(x)^{-\alpha} - 1]^{-1}\})^2. \tag{2}$$

A random variable (rv) X is said to have a PTII distribution if it has CDF (for $X > 0$) given by

$$G_{\theta,\delta} = G_{\theta,\delta}(x) = 1 - \left(\frac{x}{\delta} + 1\right)^{-\theta} |\theta > 0 \text{ and } \delta > 0, \tag{3}$$

where θ (shape) and δ (scale) are the two parameters of the model. Inserting (3) into (2), the CDF of the OGPTII model can be expressed as

$$F_{\underline{\boldsymbol{P}}}(x) = \left[1 - \beta\, exp\left(-\left\{\left[1 - \left(\frac{x}{\delta} + 1\right)^{-\theta}\right]^{-\alpha} - 1\right\}^{-1}\right)\right]^2 |\underline{\boldsymbol{P}} = \alpha, \beta, \theta, \delta. \tag{4}$$

By differentiating (4), the probability density function (PDF) of the OGPTII model can be expressed as

$$f_{\underline{\boldsymbol{P}}}(x) = 2\alpha\beta\frac{\theta}{\delta}\frac{\left[1-q_{\theta,\delta}(x)\right]^{\alpha-1} exp\left(-\left\{\left[1-q_{\theta,\delta}(x)\right]^{-\alpha}-1\right\}^{-1}\right)}{\left\{1-\left[1-q_{\theta,\delta}(x)\right]^{\alpha}\right\}^{2}\left(\frac{x}{\delta}+1\right)^{(\theta+1)}}\left[1 - \beta\, exp\left(-\left\{\left[1 - q_{\theta,\delta}(x)\right]^{-\alpha} - 1\right\}^{-1}\right)\right], \tag{5}$$

where $q_{\theta,\delta}(x) = \left(\frac{x}{\delta} + 1\right)^{-\theta}$ and $\alpha, \beta > 0$ are two additional shape parameters. For $\delta = 1$, the OGPTII reduced to the three-parameters odd-generalized Pareto Type II (TOGPTII) model. The tail index essentially tells us how heavy or light the right tail of a distribution is. A larger tail index implies a lighter tail, meaning that extreme values are less likely, while a smaller tail index indicates

a heavier tail, where large deviations from the mean are more probable. or this model, by examining the asymptotic behavior of the PDF as $x \to \infty$, we find that the dominant term behaves like

$$f_{\underline{\boldsymbol{P}}}(x) \propto \left(1 + \frac{x}{\delta}\right)^{-\theta-1}.$$

This means that the tail index of the OGPTII model is approximately $\theta + 1$. Understanding the tail behavior of the OGPTII model is especially important in industries like aviation, where reliability and safety are critical. In the case of aircraft windshield data, both failure times and service times, having a precise estimate of the tail index helps engineers and maintenance planners assess the likelihood of extreme events, such as unusually long service times or unexpected failures. With a large, estimated tail index, this model suggests that the data has a very light tail, meaning extreme values are rare, and most observations cluster around typical values. This gives confidence in designing predictive maintenance schedules without overestimating risk, helping airlines optimize costs and reduce unnecessary part replacements. At the same time, the model's flexibility allows it to capture increasing hazard rates, aligning with real system degradation over time. In short, this statistical insight enhances decision-making, improves safety protocols, and supports more efficient operations in aircraft maintenance and beyond.

Henceforth, $X \sim$OGPTII($\underline{\boldsymbol{P}}$) denotes a random variable with density function (2). Actually, several research works have built on the PTII distribution. Many of these developments were driven by the need for more flexible tools in statistical and mathematical modeling. For instance, [3] proposed a generalized version of the PTII model with useful statistical features and real applications. Figure 1 below presents different shapes of the new PDF plots (see the righ plot) and its corresponding hazard rate function (HRF) plots (see the left plot) for five selected parameter compinations for the OGPTII model. The PDF plots provide information about the likelihood of observing different values of X. The varying shapes suggest that the OGPTII model can be used for modeling a wide range of phenomena, from highly concentrated distributions to very dispersed ones. The new PDF, as depicted in Figure 1 (the left plot), exhibits characteristics of a right-skewed distribution with either a heavy tail shape or a single peak, depending on the parameter values. Figure 1 (particularly the plot on the right) demonstrates the versatility of the OGPTII model in terms of its HRF. Depending on the chosen parameters, the HRF can display a variety of shapes. These include a curve that increases and then flattens out (increasing-constant), one that rises steadily (monotonically increasing), a peaked shape that goes up and then down (upside-down or unimodal), a J-shaped curve that dips before sharply rising, and a flat line indicating a constant hazard rate over time. This range of possible forms shows how adaptable the OGPTII model is in modeling different patterns of risk or failure, making it well-suited for use in reliability and survival analysis where such variability is common.

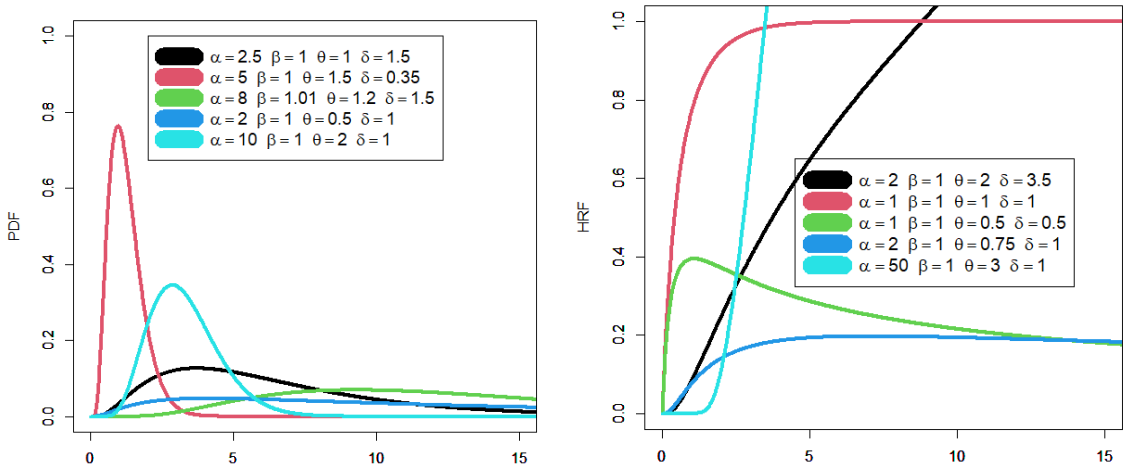

Figure 1. PDF shapes (right graph) and HRF shapes (left graph).

2. Probabilistic properties

If $u \sim u(0,1)$, then

$$x_u = \delta\left\{1-\left[1-\frac{1}{\ln\left(\frac{1-\sqrt{u}}{\beta}\right)}\right]^{-\frac{1}{\alpha}}\right\}^{-\frac{1}{\theta}}, \tag{6}$$

has CDF in (3). Following [8], the $f_{\underline{P}}(x)$ can then be expressed as

$$f_{\underline{P}}(x) = \sum_{\hbar_1,\hbar_2=0}^{\infty} C_{\hbar_1,\hbar_2}\ g_{\alpha^\bullet,\theta,\delta}(x)|\alpha^\bullet = (\hbar_1+\hbar_2+1)\alpha, \tag{7}$$

where $g_{\alpha^\bullet,\theta,\delta}(x)$ refers to the PDF of the standard exp-PTII model but with $\alpha^\bullet$ and

$$C_{\hbar_1,\hbar_2} = \frac{\alpha\beta(-1)^{\hbar_1+\hbar_2}}{\hbar_1!\,\alpha^\bullet}\binom{-(\hbar_1+2)}{\hbar_2}\sum_{j=0}^{\infty}\frac{(j+1)^{\hbar_1}(-1)^j}{\Gamma(1+j)\Gamma(2-j)}.$$

Finally, the CDF of the $g_{\alpha^\bullet,\theta,\delta}(x)$. Then

$$F_{\underline{P}}(x) = \sum_{\hbar_1,\hbar_2=0}^{\infty} C_{\hbar_1,\hbar_2}\, G_{\alpha^\bullet,\theta,\delta}(x),$$

where $G_{\alpha^\bullet,\theta,\delta}(x)$ is the CDF of the exp-PTII model with power parameter $\alpha^\bullet$. Secondly, using the result of (7) and the main results of the exp-PTII model, the rth ordinary moment of X can be derived as

$$U'_r = \sum_{\hbar_1,\hbar_2=0}^{\infty}\sum_{m=0}^{r} \Delta_{\hbar_1,\hbar_2,m}^{(r,\alpha^\bullet)}\, B\left(\alpha^\bullet, 1+\frac{m-r}{\theta}\right)|_{(\theta>r)}, \tag{8}$$

where

$$\Delta_{k_1,k_2,m}^{(r,\alpha^\bullet)} = C_{k_1,k_2}\alpha^\bullet\delta^r(-1)^m\binom{r}{m},$$

and

$$B(1+\Delta_1, 1+\Delta_2) = \int_0^1 x^{\Delta_1}(1-x)^{\Delta_2}\,dx.$$

The moment generating function (MGF) can be stated as

$$M_x(t) = \sum_{k_1,k_2=0}^{\infty}\sum_{m=0}^{r}\sum_{r=0}^{\infty}\Delta_{k_1,k_2,m,r}^{(r,\alpha^\bullet)}\,B\left(\alpha^\bullet, 1+\frac{m-r}{\theta}\right)|_{(\theta>r)}, \tag{9}$$

where

$$\Delta_{k_1,k_2,m,r}^{(r,\alpha^\bullet)} = \frac{t^r}{r!}\Delta_{k_1,k_2,m}^{(r,\alpha^\bullet)}.$$

The MGF in (8) can be used for obtaining the moments of the new model. The variance (U_2), skewness (γ_1), and kurtosis (γ_2) can be easily derived from well-known relations.

3. Estimation

While there are numerous non-Bayesian estimation techniques available in statistical literature, the method of maximum likelihood estimation (MLE) is often preferred due to its strong theoretical properties and desirable asymptotic behavior. To compute the MLE of the parameter vector $\underline{\mathbf{P}}$, we begin by constructing the log-likelihood function, which for this model takes the form:

$$\begin{aligned}\ell = \ell(\underline{\boldsymbol{P}}) &= n\,log\left(2\alpha\beta\frac{\theta}{\delta}\right) - (\theta+1)\sum_{j=1}^{n} log\left(\delta^{-1}x_j + 1\right)\\ &-2\sum_{j=1}^{n} log\left\{1-\left[1-G_{\theta,\delta}(x_j)\right]^{\alpha}\right\} + (\alpha-1)\sum_{j=1}^{n} log\left[1-G_{\theta,\delta}(x_j)\right]\\ &+\sum_{j=1}^{n} log\left[1-exp\left\{\frac{-\left[1-G_{\theta,\delta}(x_j)\right]^{\alpha}}{1-\left[1-G_{\theta,\delta}(x_j)\right]^{\alpha}}\right\}\right] + \sum_{j=1}^{n}\frac{-\left[1-G_{\theta,\delta}(x_j)\right]^{\alpha}}{1-\left[1-G_{\theta,\delta}(x_j)\right]^{\alpha}}.\end{aligned}$$

Identifying each component of the corresponding score vector, that is, the derivatives of the log-likelihood with respect to each parameter, is a straightforward process. The maximum likelihood estimates are then obtained by solving the system of nonlinear equations given by setting all partial derivatives (score functions) $U_\alpha = U_\beta = U_\theta = U_\delta = 0$ simultaneously. A critical property of any statistical model is identifiability, which ensures that different parameter values correspond to different probability distributions. For the OGPTII model, identifiability follows from the structure of the density function and the positivity of the parameters $\alpha > 0$, $\beta > 0$, $\theta > 0$, and $\delta > 0$. The functional form of the log-likelihood does not allow for distinct parameter combinations to yield the same distribution function. This was confirmed analytically by examining the score equations and numerically through simulation studies, where different parameter sets consistently produced distinct

likelihood surfaces. These properties are supported by the simulation study presented in Section 5, where the biases and mean squared errors (MSEs) of the MLEs decrease as the sample size increases, indicating convergence. The estimated sampling distributions of the MLEs also exhibit near-normality for large sample sizes, as expected. Due to the presence of multiple shape parameters, the likelihood function of the OGPTII model can be complex and potentially multimodal, especially for small or moderately sized samples.

Assessing the MLE method

In this section we will assess the MLE method via a comprehensive simulation study, the graphical simulation is chosen for its ease visual result interpretation. mean squared errors (MSE) and biases are considered for these possess. The following algorithm is considered:

1) Generate N=1500 samples of size $n|n = 50,55,60 \ldots,1000$ from the OGPTII distribution using (11).
2) Compute the MLEs for the $N = 1500$ samples.
3) Obtain the Biases and the MSE and for $h = \alpha, \beta, \theta, \delta$ and $n|_{(n=50,55,60\ldots,1000)}$.

According to Figure 2, we noted that the curve of the biases approach zero as the sample size increases and the curve of the MSEs decreases as the sample size increases. According to Figure 3, it is also seen that the curve of the biases approach zero as the sample size increases, and also the curve of the MSEs decreases as the sample size increases. According to Figure 4, it is noted that the curve of the biases approached zero as the sample size increases, and the curve of the MSEs decreases as the sample size increases and the horizontal red line shows that. According to Figure 5, we noted that the curve of the biases approach zero as the sample size increases, and the curve of the MSEs decreases as the sample size increases. Generally, the biases are negative, and it approach zero as the sample size increases. However the MSEs decreases as the sample size increases. The results of Figures 2–5 proves the efficiency of the MLE method.

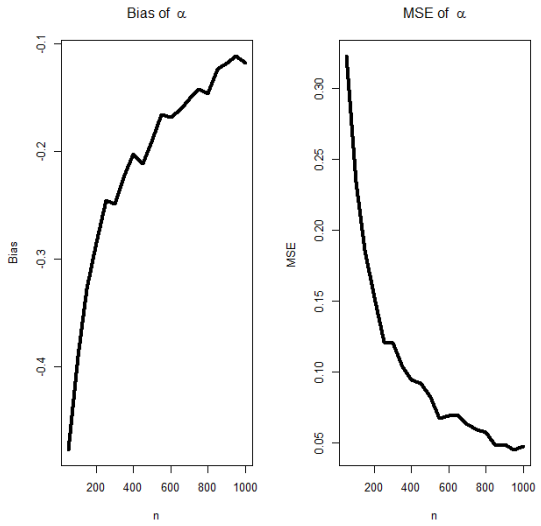

Figure 2. Biases for the parameter α (left graph)$|N = 1500;\ n = 50,55, \ldots,1000$ and MSEs for the parameter α (right graph) $|N = 1500;\ n = 50,55, \ldots,1000$.

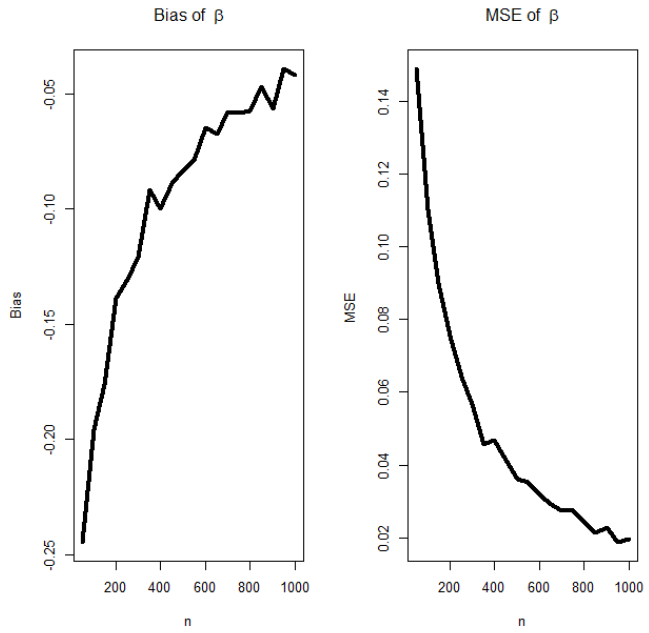

Figure 3. Biases for the parameter β (left graph)$|N = 1500;\ n = 50{,}55, \ldots{,}1000$ and MSEs for the parameter β (right graph) $|N = 1500;\ n = 50{,}55, \ldots{,}1000$.

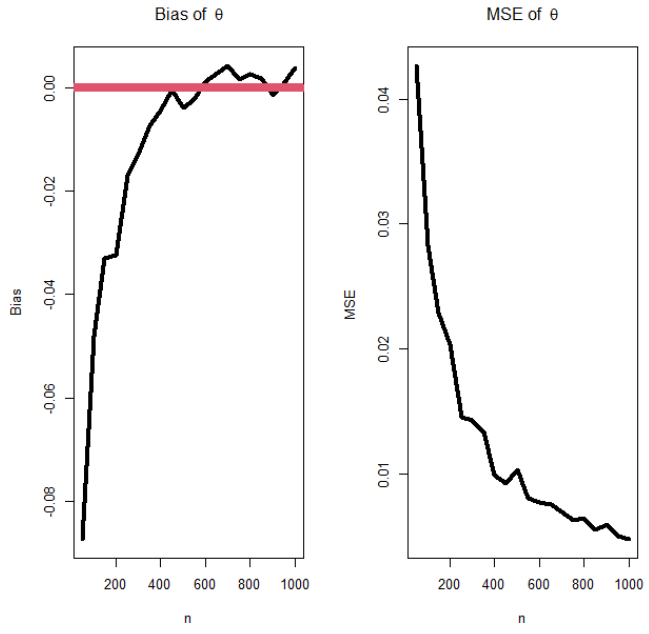

Figure 4. Biases for the parameter θ (left graph)$|N = 1500;\ n = 50{,}55, \ldots{,}1000$ and MSEs for the parameter θ (right graph) $|N = 1500;\ n = 50{,}55, \ldots{,}1000$.

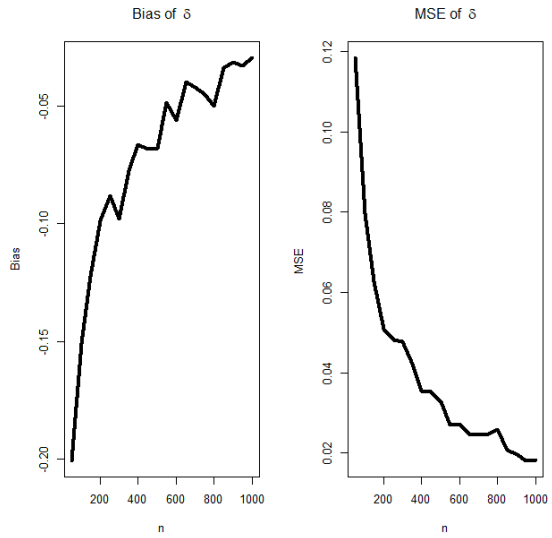

Figure 5. Biases for the parameter δ (left graph)$|N = 1500;\ n = 50{,}55, \ldots{,}1000$ and MSEs for the parameter δ (right graph) $|N = 1500;\ n = 50{,}55, \ldots{,}1000$.

4. Checking the applicability

Table 1. Competitive models.

Model	Authors
Three-parameters odd-generalized Pareto Type II TOGPTII)	New
Special generalized mixture PTII (SGMPTII)	[9]
Kumaraswamy-PTII (KPTII)	[10]
Beta-PTII (BPTII)	[10]
PTII	[11]
Burr-Hatke-PTII (BHPTII)	[12]
Odd-loglogistic-PTII (OLLPTII)	[13]
Transmute-Topp-Leone PTII (TTLPTII)	[14]
Reduced TTLPTII (RTTLPTII)	[14]
Proportional reversed hazard rate PTII (PRHRPTII)	-
Generalized odd generalized exponential PTII (GOGEPTII)	[15]
Reduced- GOGEPTII (GOGEPTII)	[15]
Reduced-OLLPTII (R-OLLPTII)	[13]
Exponentiated-PTII (Exp-PTII)	[16]
Reduced-Burr-Hatke-PTII (R-BHPTII)	[12]

When working with high-value datasets, it is essential to choose a distribution that accurately reflects the underlying data. This typically involves using both statistical tests and graphical tools to assess how well different models fit the observed data. In this section, however, we turn our attention to two real-life datasets that do not contain extreme values. These datasets are used in distinct application settings to demonstrate the relevance, adaptability, and performance of the OGPTII model in contexts where extreme observations are absent. To evaluate its effectiveness, we compare

the OGPTII model's fit against several well-established competing distributions. Table 1 provides an overview of several models that have been proposed as generalizations or modifications of the classic Pareto Type II (PTII) distribution.

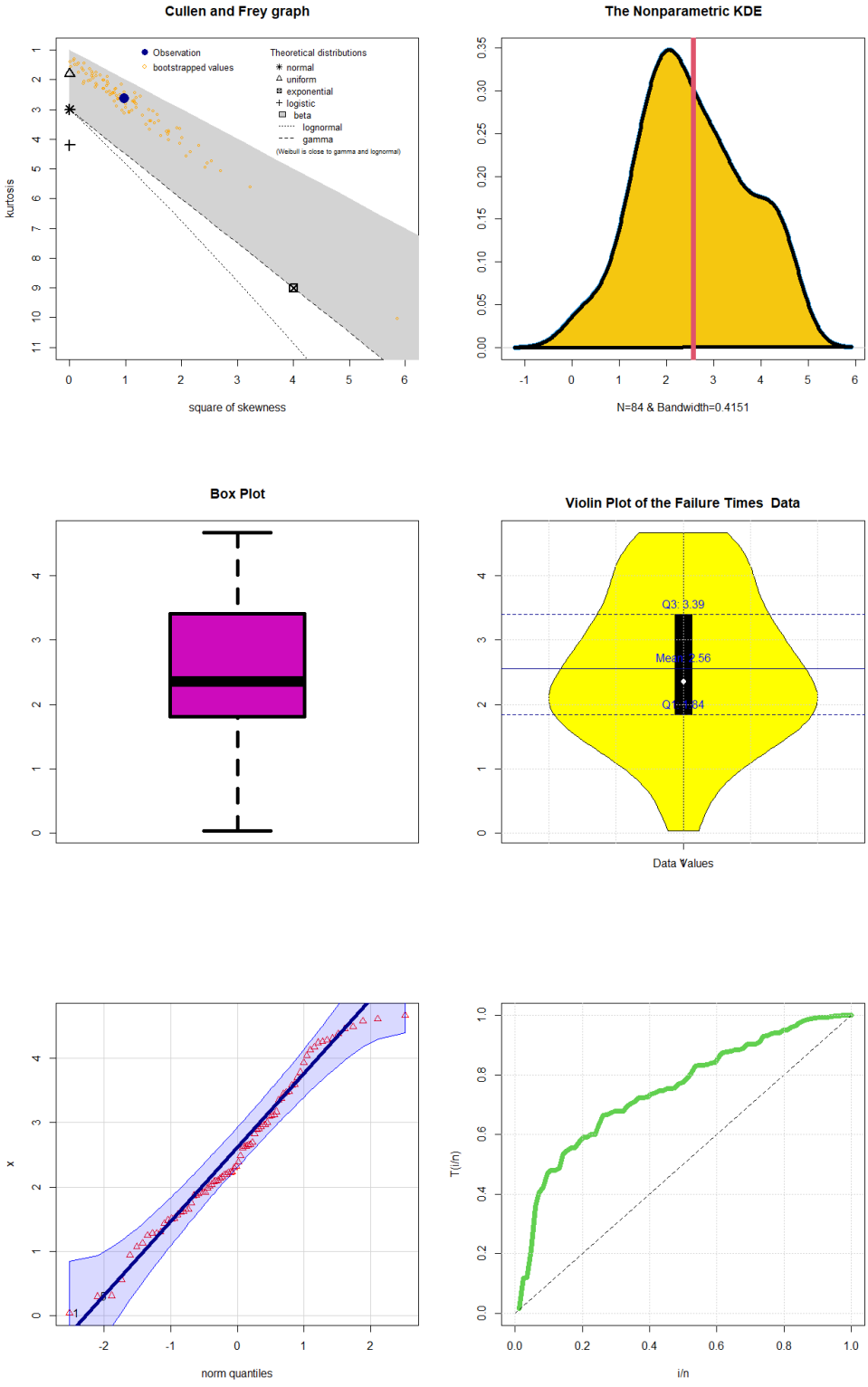

Figure 6. Cullen and Frey plot, nonparametric KDE plot, box plot, violin plot, Q-Q plot, TTT for the failure data.

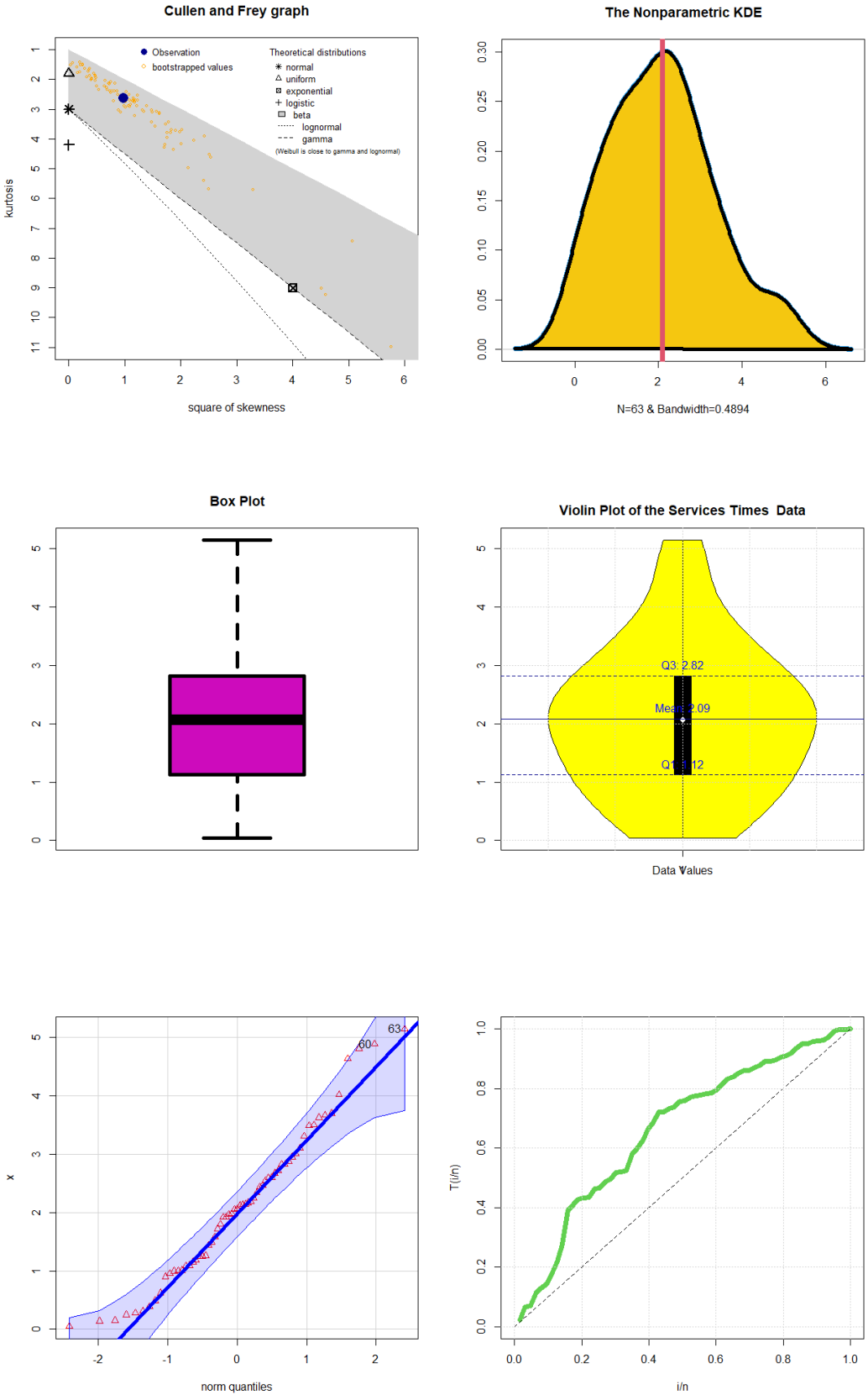

Figure 7. Cullen and Frey plot, nonparametric KDE plot, box plot, violin plot, Q-Q plot, TTT for the service times data.

First dataset: The first real-world data set consists of recorded "failure times" for 84 aircraft windshields, originally reported in [17]. This data set, referred to as dataset I, provides actual lifetime observations and serves as a practical example for modeling failure behavior. Second dataset: The second real-world data set, labeled as dataset II, contains information on the "service times" of 63 aircraft windshields. It also comes from the same source, [17], and is used to evaluate the performance of the proposed model in capturing service-life patterns. Figure 6 below presents the Cullen and Frey plot, the nonparametric kernel density estimation (KDE) plot, box plot, Violin plot, quantile-quantile (Q-Q) plot, and the total time in test (TTT) for the reliability dataset I. Looking at Figure 6, we can clearly see that the data follows a right-skewed pattern with heavier tails, which is well-captured in the Cullen and Frey plot, and KDE plot, and confirmed again in the box and violin plots. The Q-Q plot further supports this by showing clear deviation from normality, reinforcing that traditional Gaussian assumptions will not work here. The TTT plot suggests an increasing HRF over time, which makes sense for real failure time data where wear-out or fatigue plays a role.

Figure 7 presents the Cullen and Frey plot, nonparametric KDE plot, box plot, violin plot, Q-Q plot, the TTT for the services times dataset, Figure 7 clearly provides a comprehensive visual analysis of the service times dataset , much like Figure 6 did for failure times. The plots in Figure 7 collectively show that the service times data is also right-skewed and possibly heavy-tailed , similar dataset I. The KDE and violin plots confirm the skewness, while the Q-Q plot deviates from the reference line, indicating non-normality and ruling out Gaussian assumptions. The box plot shows no extreme outliers, which suggests the data is consistent and reliable. Finally, the TTT plot appears slightly concave, suggesting an increasing hazard rate over time , which is common in systems where wear-out or fatigue occurs with prolonged use. All these observations strongly support the use of a flexible model like the OGPTII to accurately represent the service times data.

The tail index of the OGPTII model is derived from its asymptotic behavior, where the probability density function exhibits a power-law decay. By analyzing the given PDF and focusing on the dominant terms as $x \to \infty$, it becomes evident that the tail index is determined by the parameter θ, with the tail index being $\theta + 1$. This indicates that the distribution possesses heavy tails, which are essential for modeling extreme events or rare occurrences such as financial crashes, insurance losses, or mechanical failures. The estimated value of the tail index, using the MLE estimates from Table 2 results in a tail index of approximately 142.586, suggesting relatively light-tailed behavior compared to classical heavy-tailed distributions but still allowing for flexibility in capturing real-life variability. This makes the OGPTII model particularly suitable for applications in finance, insurance, and reliability engineering, where understanding tail risk is crucial. The estimated value of θ=10153.7 for the OGPTII model fitted to the service times dataset leads to a tail index of approximately 10154, indicating a very light-tailed distribution. This supports the use of the model in contexts where data shows moderate variability and extreme events are rare, aligning well with real-life service time behavior in systems like aircraft windshield maintenance.

For comparing the applicability and flexibility of all models, we considered the negative log-likelihood (-ℓ), Akaike Information Criterion (AINC), Bayesian Information Criterion (BINC), Hannan-Quinn Information Criterion (HQIC), and other test statistics like Anderson-Darling (ADg), Cramér-von Mises (CVMs), and Kolmogorov-Smirnov (KS), with corresponding p-values. Table 2 presents the MLEs and their corresponding SEs for various probability models fitted to the "failure times" dataset. It includes several generalized Pareto Type II (PTII) models, namely the OGPTII (the new model), GOGEPTII, TTLPTII, KPTII, BPTII, TOGPTII, RGOGEPTII, PRHRPTII, RTTLPTII, SGMPTII, OLLPTII, BHPTII, Exp-PTII, R-OLLPTII, R-BHPTII, and PTII. The values indicate how

each model's parameters are estimated according to the data, with the SEs providing a measure of uncertainty around these estimates.

Table 2. The MLEs and SEs for failure data.

Model	MLEs (SEs)			
OGPTII($\alpha,\beta,\theta,\delta$)	1.35385	0.94577	141.586	349.074
	(2.631e-01)	(4.61e-02)	(5.15e+02)	(1.29e+03)
GOGEPTII($\alpha,\beta,\theta,\delta$)	2.251053	1.105984	6254.022	13008.314
	(1.834741)	(0.742381)	(1836.74)	(573.4623)
TTLPTII($\alpha,\beta,\theta,\delta$)	-0.807523	2.47662	(15608.4)	(386228.3)
	(0.13962)	(0.54177)	(1602.38)	(123.9431)
KPTII($\alpha,\beta,\theta,\delta$)	2.615044	100.2761	5.27719	78.67757
	(0.382262)	(120.4881)	(9.81174)	(186.4119)
BPTII($\alpha,\beta,\theta,\delta$)	3.603604	33.63876	4.83071	118.8745
	(0.61873)	(63.71451)	(9.23812)	(428.9933)
TOGPTII(α,β,θ)	3.4504609	0.9387497	1.5097833	
	(0.710225)	(0.03992)	(0.13945)	
RGOGEPTII(α,β,θ)	2.135891	2.199072	1.241233	
	(1.012476)	(0.88624)	(0.22173)	
PRHRPTII(α,θ,δ)	3.7231×10^{6}	4.712×10^{-1}	4.54×10^{6}	
	1.3124×10^{6}	(0.000114)	37.14701	
RTTLPTII(α,θ,δ)	-0.847323	5.520575	1.156784	
	(0.100109)	(1.184793)	(0.09594)	
SGMPTII(α,θ,δ)	-1.044×10^{-1}	9.8313×10^{6}	1.184×10^{7}	
	(0.122235)	(4843.353)	(501.0431)	
OLLPTII(α,θ,δ)	2.3263613	(7.171×10^{5})	2.3422×10^{6})	
	(2.143×10^{-1})	(1.149×10^{4})	(2.616×10^{1})	
BHPTII(α,θ,δ)	3.587604	52001.496	37029.666	
	(0.513331)	(7955.02)	(81.16443)	
Exp-PTII(α,θ,δ)	3.626104	20074.56	26257.685	
	(0.6236124)	(2041.8313)	(99.741771)	
R-OLLPTII(α,θ)	3.8905646	0.57316436		
	(0.365246)	(0.019466)		
R-BHPTII(α,θ)	10801754.5	513670891.3		
	(9833192.4)	(2323222.7)		
PTII(θ,δ)	51425.365	131789.615		
	(5932.4922)	(296.01935)		

Table 3 presents various goodness-of-fit statistics for different probability models applied to the dataset I. The OGPTII model shows the best performance overall, with the lowest -ℓ and information criteria values. Other models, such as GOGEPTII and OLLPTII, also perform reasonably well but not as consistently as OGPTII. Notably, the p-values from the KS test suggest that several models are statistically acceptable, but OGPTII has the highest p-value, indicating a superior fit. This table is crucial for selecting the most appropriate model for modeling failure time data in reliability studies.

Looking at the results of Table 3, it is clear that the OGPTII model outperforms all other models in terms of fit quality. Its low -ℓ value suggests it captures the underlying data structure more effectively than the others. The AINC, BINC, and HQIC values reinforce this conclusion, making OGPTII the top choice for this dataset. While some competing models like GOGEPTII and OLLPTII show decent performance, their higher criterion values indicate less efficiency. The high p-value from the KS test for OGPTII further confirms its adequacy, showing that the model closely represents the true data distribution. This strong statistical support makes OGPTII a reliable option for modeling failure times in engineering and reliability contexts. Overall, these findings highlight the importance of choosing flexible and well-fitting models when analyzing real-life data.

Table 3. Results of the -ℓ and other statistics for failure data.

Model	-ℓ	AINC	C-AINC	BINC	HNQIC	ADg	CVMs	KS(P-vale)
OGPTII	127.9841	263.9683	264.4746	273.6915	267.877	0.4553	0.0554	0.0619(0.9040)
GOGEPTII	129.6054	267.2108	267.7172	276.9341	271.1195	0.6334	0.0705	0.0716(0.8716)
OLLPTII	134.4234	274.8472	275.1472	282.1395	277.7786	0.9406	0.1008	0.0776(0.7823)
KPTII	134.5553	275.0121	276.1981	283.9825	278.1153	0.9554	0.1114	0.0673(0.7925)
TOGPTII	135.3985	276.796	277.092	284.0885	279.7278	0.05963	0.6408	0.10144(0.3538)
TTLPTII	135.5704	279.1407	279.6465	288.8637	283.0489	1.1256	0.1275	0.0793(0.7205)
BHPTII	138.4045	282.8084	283.1045	290.1365	285.7557	1.3665	0.1616	0.0802(0.7197)
BPTII	138.7178	285.4354	285.9355	295.2064	289.3655	1.4085	0.1687	0.0835(0.7196)
RGOGEPTII	140.2267	286.4527	286.7526	293.7456	289.3848	1.7385	0.2176	0.13283(0.1026)
Exp-PTII	141.3992	288.7994	289.0956	296.1273	291.7466	1.7436	0.2193	0.0861(0.7184)
R-OLLPTII	142.8454	289.6905	289.8384	294.5523	291.6444	1.9563	0.2552	0.0904(0.7185)
SGMPTII	143.0871	292.1743	292.4746	299.4674	295.1064	1.3462	0.1575	0.0924(0.7185)
RTTLPTII	153.9807	313.9615	314.2613	321.2543	316.8935	3.7526	0.5593	0.0933(0.7174)
PRHRPTII	162.8775	331.7544	332.0545	339.0467	334.6859	1.3677	0.1605	0.0953(0.7154)
PTII	164.9885	333.9764	334.1232	338.8624	335.9415	1.3974	0.1663	0.0945(0.7135)
R-BHPTII	168.6044	341.2085	341.3566	346.0657	343.1644	1.6741	0.2066	0.0974(0.7119)

Table 4 presents the MLEs and their corresponding SEs for various models fitted to the dataset II. It includes several generalized Pareto Type II (PTII) models such as OGPTII, GOGEPTII, BPTII, TTLPTII, KPTII, TOGPTII, RGOGEPTII, PRHRPTII, SGMPTII, OLLPTII, BHPTII, Exp-PTII, R-OLLPTII, R-BHPTII, and PTII. The values indicate how each model's parameters are estimated based on the service times data.

Table 4. MLEs and SEs for service data.

Model	MLEs (SEs)			
OGPTII($\alpha,\beta,\theta,\delta$)	7.42122×10^{-1}	9.481255×10^{-1}	1.01537×10^{4}	3.415558×10^{4}
	(1.744×10^{-1})	(7.780×10^{-2})	(112.363)	(324.241)
GOGEPTII($\alpha,\beta,\theta,\delta$)	2.546133	0.5937234	110.2576	224.61935
	(0.627633)	(0.094727)	(623.0144)	(450.5225)
BPTII($\alpha,\beta,\theta,\delta$)	1.921815	30.999483	4.968425	168.5734
	(0.31845)	(316.8214)	(50.5289)	(330.229)
TTLPTII($\alpha,\beta,\theta,\delta$)	(-0.62772)	1.7828821	2122.343	4823.788
	(0.213713)	(0.415224)	(163.9124)	(200.239)
KPTII($\alpha,\beta,\theta,\delta$)	1.669154	60.56755	2.564915	64.06408
	(0.257223)	(86.01331)	(4.758937)	(176.595)
TOGPTII(α,β,θ)	1.6073325	0.9082026	1.1110658	
	(0.386712)	(0.060399)	(0.156197)	
RGOGEPTII(α,β,θ)	2.027826	1.222992	1.167529	
	(1.194413)	(0.601433)	(0.2705403)	
PRHRPTII(α,θ,δ)	1.66667×10^{6}	3.8998×10^{-1}	1.3388×10^{6}	
	2.1121×10^{3}	0.00114×10^{-1}	0.9851×10^{6}	
RTTLPTII(α,θ,δ)	-0.6714215	2.7449621	1.0123814	
	(0.187464)	(0.669615)	(0.1140511)	
SGMPTII(α,θ,δ)	-1.0444×10^{-1}	6.4541×10^{6}	6.3344×10^{6}	
	($4.135\times e^{-10}$)	(3.2147×10^{6})	(3.854737)	
OLLPTII(α,θ,δ)	1.6641934	6.3484×10^{5}	2.0154×10^{6}	
	(1.796×10^{-1})	(1.736×10^{4})	7.2526×10^{6}	
BHPTII (α,θ,δ)	1.9073236	35842.4336	39197.5567	
	(0.321324)	(6945.473)	(151.6543)	
Exp-PTII(α,θ,δ)	1.9145354	22971.158	32881.998	
	(0.34824)	(3209.555)	(162.2304)	
R-OLLPTII(α,θ)	2.372333	0.691239		
	(0.268243)	(0.044935)		
R-BHPTII(α,θ)	14055542	53203443		
	(422.0435)	(28.52313)		
PTII(θ,δ)	99269.85	207019.46		
	(11863.53)	(301.2373)		

Table 5 presents the goodness-of-fit statistics for various probability models applied to the dataset II. This data is crucial for selecting the most appropriate model for modeling service time data in reliability studies. Looking at the results of Table 5, the OGPTII model outperforms all other models in terms of fit quality for the dataset II. Its low -ℓ value suggests it captures the underlying data structure more effectively than the others. The AINC, BINC, and HQIC values reinforce this conclusion, making OGPTII the top choice for this dataset. While some competing models like GOGEPTII and KPTII show decent performance, their higher criterion values indicate less efficiency. The moderate p-value from the KS test for the OGPTII further confirms its adequacy, showing that the model closely represents the true data distribution. This strong statistical support makes OGPTII a reliable option for modeling service times in engineering and reliability contexts.

Table 5. Results of the -ℓ and other statistics for service data.

Model	-ℓ	AINC	C-AINC	BINC	HNQIC	ADg	CVMs	KS(P-vale)
OGPTII	98.81637	205.6327	206.3224	214.2053	209.0044	0.2921	0.0451	0.0836(0.7384)
GOGEPTII	98.92234	206.5343	206.5343	214.4172	209.2163	0.4389	0.0721	0.0995(0.5273)
KPTII	100.8677	209.7355	210.4248	218.3079	213.1066	0.7396	0.1218	0.1002(0. 7378)
TTLPTII	102.4499	212.8999	213.5894	221.4723	216.2715	0.9434	0.1556	0.1006(0. 7259)
BHPTII	102.8336	211.6665	212.0733	218.0998	214.1959	1.1125	0.1837	0.1019(0. 7158)
SGMPTII	102.8944	211.7886	212.1944	218.2173	214.3169	1.1136	0.1835	0.1007(0. 7157)
BPTII	102.9615	213.9253	214.6159	222.4938	217.2969	1.1386	0.1892	0.1032(0. 7011)
TOGPTII	103.0922	212.1838	212.5916	218.6352	214.7165	0.82962	0.1318	0.13848(0.1607)
Exp-PTII	103.5499	213.0994	213.5065	219.5299	215.6289	1.2381	0.2047	0.1008(0. 7033)
RGOGEPTII	104.1286	214.2574	214.6651	220.6868	216.788	1.3255	0.2205	0.16441(0.0585)
OLLPTII	104.9042	215.8083	216.2350	222.2373	218.3379	0.974	0.1547	0.1007(0.6976)
PRHRPTII	109.2984	224.5974	225.044	231.0265	227.128	1.1266	0.1862	0.1007 (0.6946)
PTII	109.2987	222.5975	222.7973	226.8859	224.2844	1.1266	0.1866	0.1007 (0.6955)
R-OLLPTII	110.7288	225.4575	225.6574	229.7456	227.1436	2.3474	0.3918	0.1008 (0.6021)
RTTLPTII	112.1856	230.3760	230.7668	236.8664	232.8967	2.6876	0.4535	0.1009(0.58821)

For both the datasets, Figures 8 and 9 display the estimated Kaplan–Meier survival function (EKMSF), the estimated probability density function (EPDF), the estimated cumulative distribution function (ECDF), and the probability–probability (P–P) plots. When considered alongside Tables 3 and 5, these visual tools clearly demonstrate the broad flexibility and strong fitting capability of the proposed model.

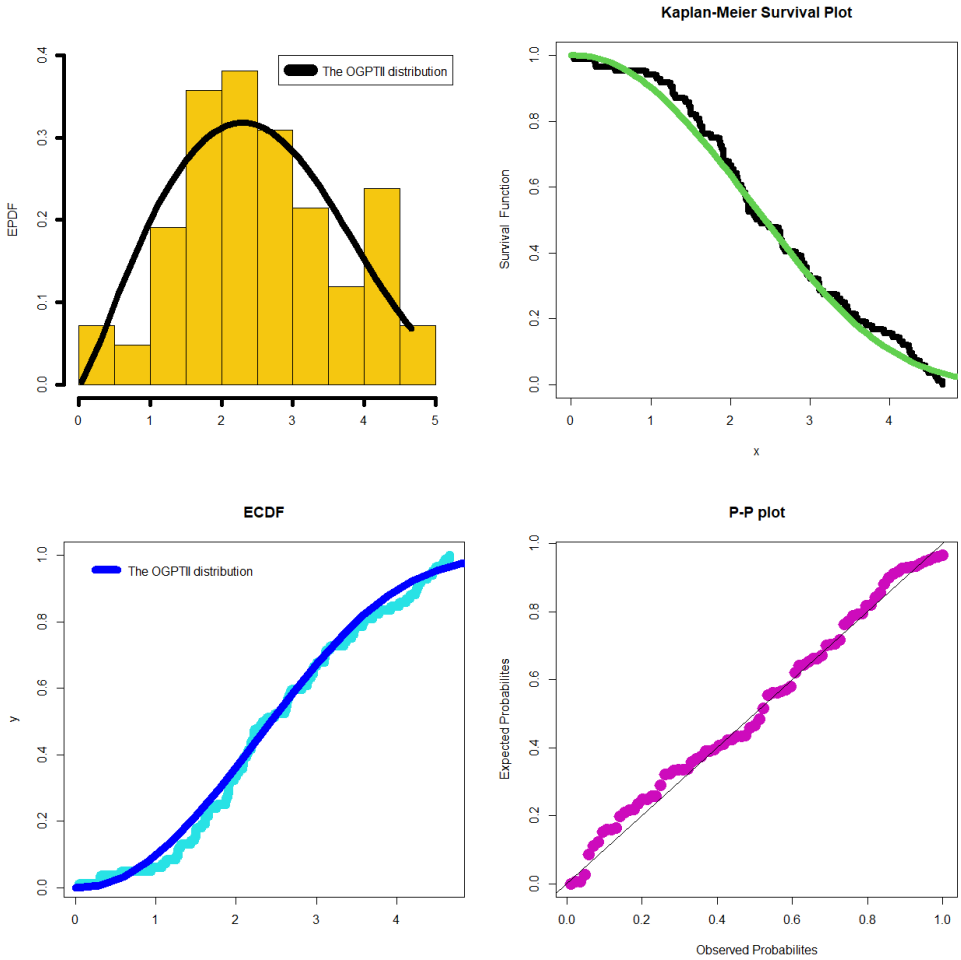

Figure 8. EPDF plot, EKMSF plot, ECDF plot and P-P plot plot for data set I.

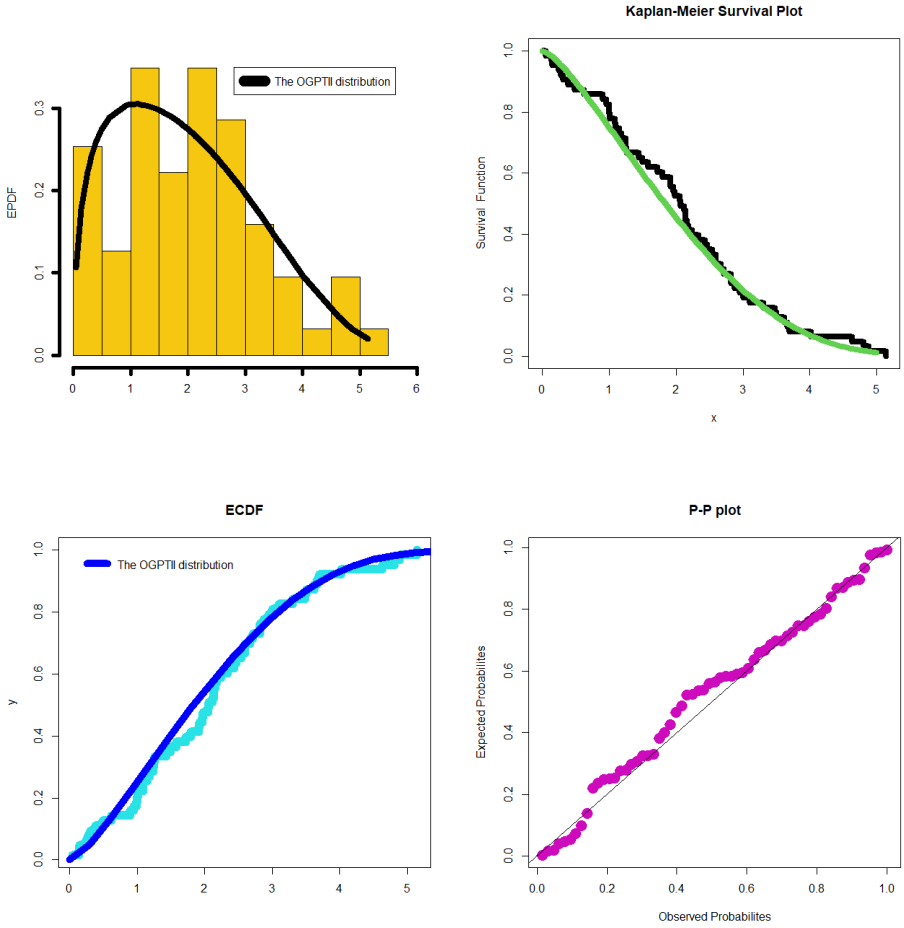

Figure 9. EPDF plot, EKMSF plot, ECDF plot and P-P plot plot for data set II.

5. Two reliability engineering case studies

Reliability engineering is essential for ensuring the safety, performance, and durability of critical systems, especially in high-stakes environments like aviation. One of the key challenges in this field lies in accurately modeling failure and service times to predict system behavior, optimize maintenance schedules, and reduce the risks associated with unexpected failures. Traditional statistical models often struggle when dealing with real-life data that exhibit non-standard patterns, such as varying hazard rates or heavy-tailed distributions. Therefore, developing more flexible and robust statistical models is crucial for advancing reliability analysis.

In this section, we present two detailed case studies focused on aircraft windshield reliability using the newly proposed OGPTII model. The aircraft windshields are vital components that must endure significant mechanical and environmental stress during flight operations. Understanding their failure and service time characteristics is essential for developing predictive maintenance strategies and ensuring operational safety. The OGPTII model, with its enhanced flexibility, offers a powerful framework for analyzing these reliability metrics by capturing a wide range of hazard rate shapes. The first case study investigates failure time data from 84 aircraft windshields, while the second focuses on

service time data for the same set of windshields. Both datasets are analyzed using the OGPTII model and compared against several well-established reliability models. We apply advanced statistical tools, such as the Hill estimator, MOOP, VaR, TVaR, and PORT analysis, to assess tail behavior, quantify risk, and evaluate the model's ability to capture extreme events.

These case studies demonstrate the superior fitting capability of the OGPTII model and highlight its practical relevance in identifying potential risk factors and informing decision-making processes in reliability engineering. By providing accurate estimates of failure probabilities and service life expectations, the OGPTII model supports the design of cost-effective maintenance protocols and enhances overall system resilience. The insights gained from these analyses underscore the importance of adopting advanced statistical models in modern reliability engineering practices. Figure 10 provides the nonparametric Hill plot (tail index vs. number on the top observations) and the stability plot for the dataset I. Figure 11 shows the nonparametric Hill plot (tail index vs number on the top observations) and the stability plot for the dataset II. Together, Figures 10 and 11 proof that the tail of the two data sets can be estimated by our new model.

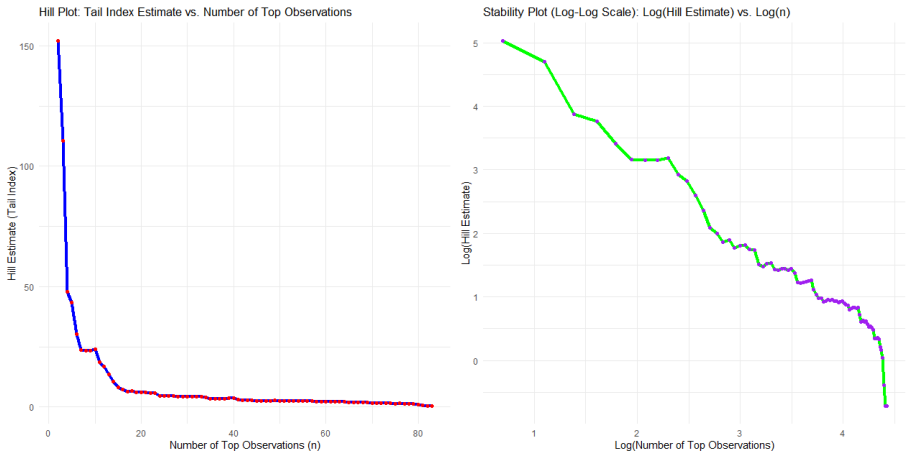

Figure 10. The nonparametric Hill plot (tail index vs. number on the top observations) and the stability plot for the dataset I.

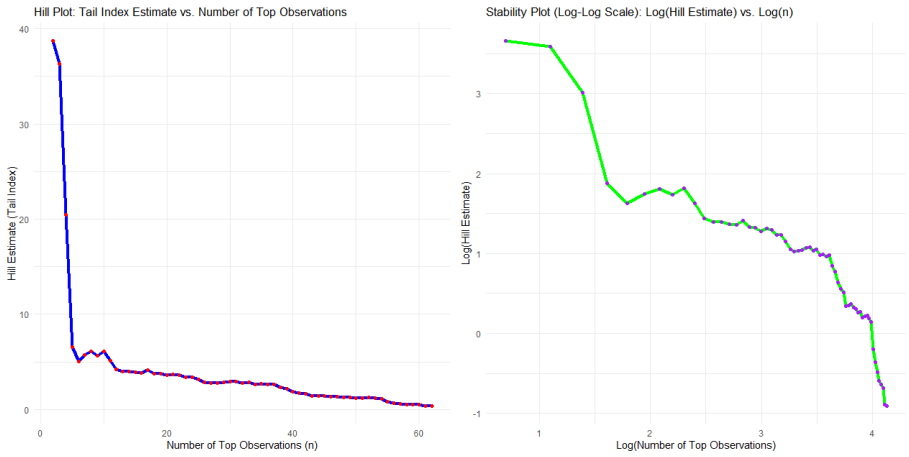

Figure 11. The nonparametric Hill plot (tail index vs. number on the top observations) and the stability plot for the dataset II.

Table 6 (part I) summarizes how MOOP estimates the failure and service times of aircraft windshields for increasing values of P from 1 to 55. The true mean failure and service times are 2.557 and 2.085, respectively. As PP increases, MOOP values grow for failure times from 0.040 (P=1) to 0.430 (P=5), and for service times from 0.046 to 0.173. Both MSE and bias show a decreasing trend, signaling more accurate approximations of the true mean. The Hill estimators are very small (0.0070 for failure, ~0.0001 for service), pointing to light-tailed distributions. In the field of reliability engineering for aircraft windshields, accurate modeling of failure and service times is crucial for safety and maintenance planning. At low orders (e.g., P=1), the MOOP significantly underestimates the mean, just 0.040 for failure times versus the true value of 2.557, with a high bias of 2.517. By increasing P to 5, MOOP for failure time rises to 0.430, reducing the bias to 2.127 and the MSE from 6.338 to 4.526. Similarly, for service times, MOOP improves from 0.046 to 0.173, and the bias drops from 2.039 to 1.912. This steady improvement confirms that higher-order means are more effective at capturing the core behavior of reliability metrics. The low Hill estimator (0.007 for failure, nearly 0 for service) shows both variables have very light tails, suggesting low risk of extreme or sudden breakdowns. Such insight supports confidence in planned maintenance cycles rather than emergency responses. From a practical standpoint, it means fewer surprises in operational readiness and better cost-efficiency in windshield upkeep. Moreover, identifying the right-order P balances estimation precision with sensitivity to rare events. These results reinforce the value of tailored statistical tools like MOOP for improving aircraft reliability models.

Part II of Table 6 reports four key risk indicators: VaR, Tail Value-at-Risk (TVaR), Tail Variance Contribution (TVc), and Tail Mean-Variance (TMVc), for both failure and service times of aircraft windshields across confidence levels (CL) from 0.55 to 0.95. As CL increases, the values of VaR and TVaR for both failure and service times decrease, reflecting a lower frequency but higher severity of rare events. TVc increases with CL, capturing more weight in the distribution's extreme right tail. TMVc stays relatively stable, with minor reductions as CL grows, especially for service times. This analysis may help identify how risk exposure evolves under increasing certainty levels in reliability analysis.

In aircraft windshield reliability, managing risk under uncertainty is just as important as predicting mean failure times. The VaR for failure times drops from 2.223 at CL=0.55 to 0.943 at CL=0.95, indicating that the maximum expected failure time under normal conditions reduces as we look further into the tail. The TVaR for failures shrinks from 3.370 to 2.692, showing reduced expected losses beyond VaR but still accounting for rare, extreme scenarios. For service times, the VaR drops from 1.963 to 0.248, a sharp decline that flags the system’s vulnerability to underestimation at higher confidence levels. However, TVc increases across both categories (from 0.557 to 1.018 for failure, and 0.783 to 1.380 for service), highlighting that tail contributions grow as we look further into risk extremes. This shift suggests that more of the "risk weight" is hidden in the tails, a critical insight for safety engineers. The TMVc, especially for failure times (ranging from 3.927 to 3.710), remains relatively flat, signaling stable mean-variance structure even as tail behavior changes. This consistency implies that while extremes vary, the average volatility structure of failures doesn't fluctuate dramatically, which is vital for maintenance planning.

Part III of Table 6 shows the PORT analysis for failure and service times of aircraft windshields across confidence levels (CL = 0.55 to 0.95). For each CL, the table lists the threshold, number of peaks above VaR (NP), and the resulting PORT value. As CL increases, thresholds rise, and so does the number of exceedances, e.g., for failure times, NP rises from 46 to 79. However, PORT values

decreased steadily, e.g., from 0.9449 to 0.1158 for failure times, indicating fewer extreme events per exceedance. This dynamic reflects how risk sharpens in the tail, even as fewer observations lie above an ever-rising threshold.

Table 6. MOOP analysis for P=1,2,3,4,5, risk indicators, and PORT analysis under some CL values.

Part	Analysis	Failure times for the aircraft windshields	Service times for the aircraft windshields
I	True Mean	2.557	2.085
	MOOP|P=1,2,3,4,5	0.040; 0.171; 0.217; 0.302; 0.430	0.046; 0.093; 0.112; 0.146; 0.173
	MSE|P=1,2,3,4,5	6.338, 5.698; 5.479; 5.088; 4.526	4.159; 3.969; 3.893; 3.761; 3.657
	Bias|P=1,2,3,4,5	2.517; 2.387; 2.341; 2.256; 2.127	2.039; 1.993; 1.973; 1.939; 1.912
	Hill estimator	0.0070133	9.849×10^{-5}
II	CL ↓and risk indicator→	VaR; TVaR; TVc; MVc	VaR; TVaR; TVc; TMVc
	0.55	2.223; 3.370; 0.557; 3.927	1.963 2.993 0.783 3.775
	0.60	2.135; 3.275; 0.616; 3.891	1.794 2.907 0.804 3.710
	0.65	2.038; 3.188; 0.666; 3.854	1.492 2.816 0.846 3.662
	0.70	1.912; 3.106; 0.714; 3.819	1.244 2.684 0.948 3.632
	0.75	1.757; 3.009; 0.765; 3.775	1.092 2.588 1.022 3.610
	0.80	1.615; 2.929; 0.821; 3.751	1.003 2.497 1.093 3.590
	0.85	1.480; 2.852; 0.877; 3.729	0.900 2.411 1.155 3.566
	0.90	1.281; 2.793; 0.924; 3.717	0.389 2.318 1.250 3.568
	0.95	0.943; 2.692; 1.018; 3.710	0.248 2.217 1.380 3.597
III	CL ↓and PORT analysis →	Threshold; NP above VaR; PORT	Threshold; NP above VaR; PORT
	0.55	2.6296; 46; 0.9449	2.1432; 35; 1.0446
	0.60	2.7960; 50; 0.8865	2.2602; 38; 1.0467
	0.65	2.9606; 54; 0.8279	2.4877; 41; 0.9411
	0.70	3.1143; 59; 0.8262	2.6280; 44; 0.9351
	0.75	3.3927; 63; 0.6791	2.8195; 47; 0.8988
	0.80	3.5848; 67; 0.6236	2.9818; 50; 0.9293
	0.85	3.9850; 71; 0.3646	3.4293; 53; 0.7142
	0.90	4.2505; 74; 0.1921	3.6564; 56; 0.7479
	0.90	4.4380; 79; 0.1158	4.5667; 59; 0.2971

In reliability engineering for aircraft windshields, PORT analysis plays a critical role in identifying rare, high-impact failure events. A key finding is that while the number of exceedances above VaR grows with confidence level (from 46 to 79 for failures), the PORT values shrink, from 0.9449 down to just 0.1158. This indicates that as we look deeper into the tail (higher thresholds), events become more clustered but less individually extreme, typical of light-tailed phenomena. For service times, a similar pattern emerges: NP increases from 35 to 59, while PORT drops from 1.0446 to 0.2971. From an engineering perspective, this means that service disruptions, while still occurring, become more predictable and containable at higher risk thresholds. The rising thresholds (e.g., failure

threshold from 2.6296 to 4.4380) show how rare it is to reach extreme states, further reinforcing design confidence. These trends suggest that the windshield systems are well within operational resilience limits, and maintenance protocols can be planned rather than reactive. The low PORT values at high CLs support the idea that extreme failures are not just rare but also mild in intensity. This enables engineers to allocate resources more effectively, focusing not on rare catastrophes, but on maintaining consistent performance. Ultimately, PORT gives engineers a quantitative lens to understand and prepare for worst-case reliability events without overestimating risk. Figure 12 provides the histograms of threshold; NP above VaR; and PORT for the failure times for the aircraft windshields. Figure 13 presents the KDE of threshold; NP above VaR; and PORT for the failure times for the aircraft windshields. Figure 14 shows the histograms of threshold; NP above VaR; and PORT for the service times for the aircraft windshields. Figure 15 illustrates the KDE of threshold; NP above VaR; and PORT for the service times for the aircraft windshields. Figures 12–15 are plotted based on the results of Table 6.

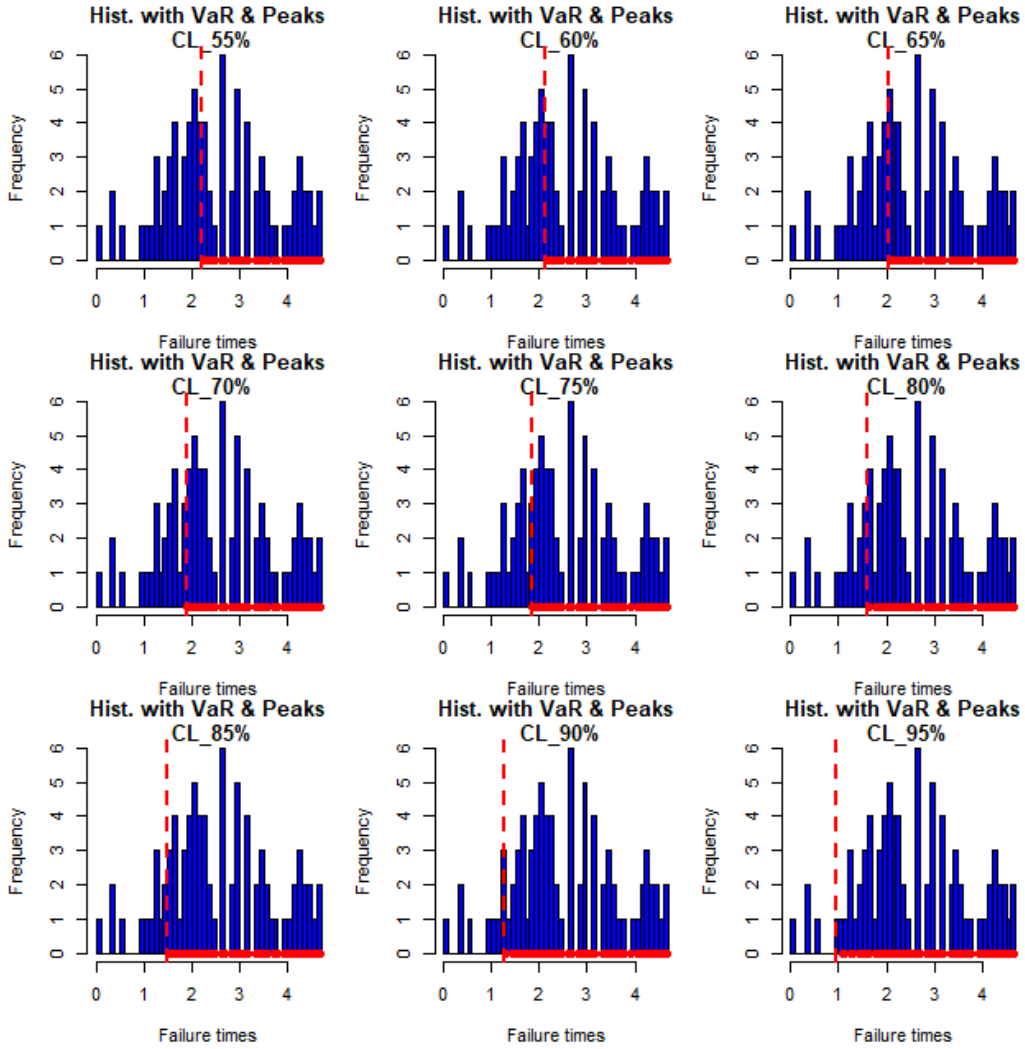

Figure 12. Histograms of threshold; NP above VaR; PORT for the failure times for the aircraft windshields.

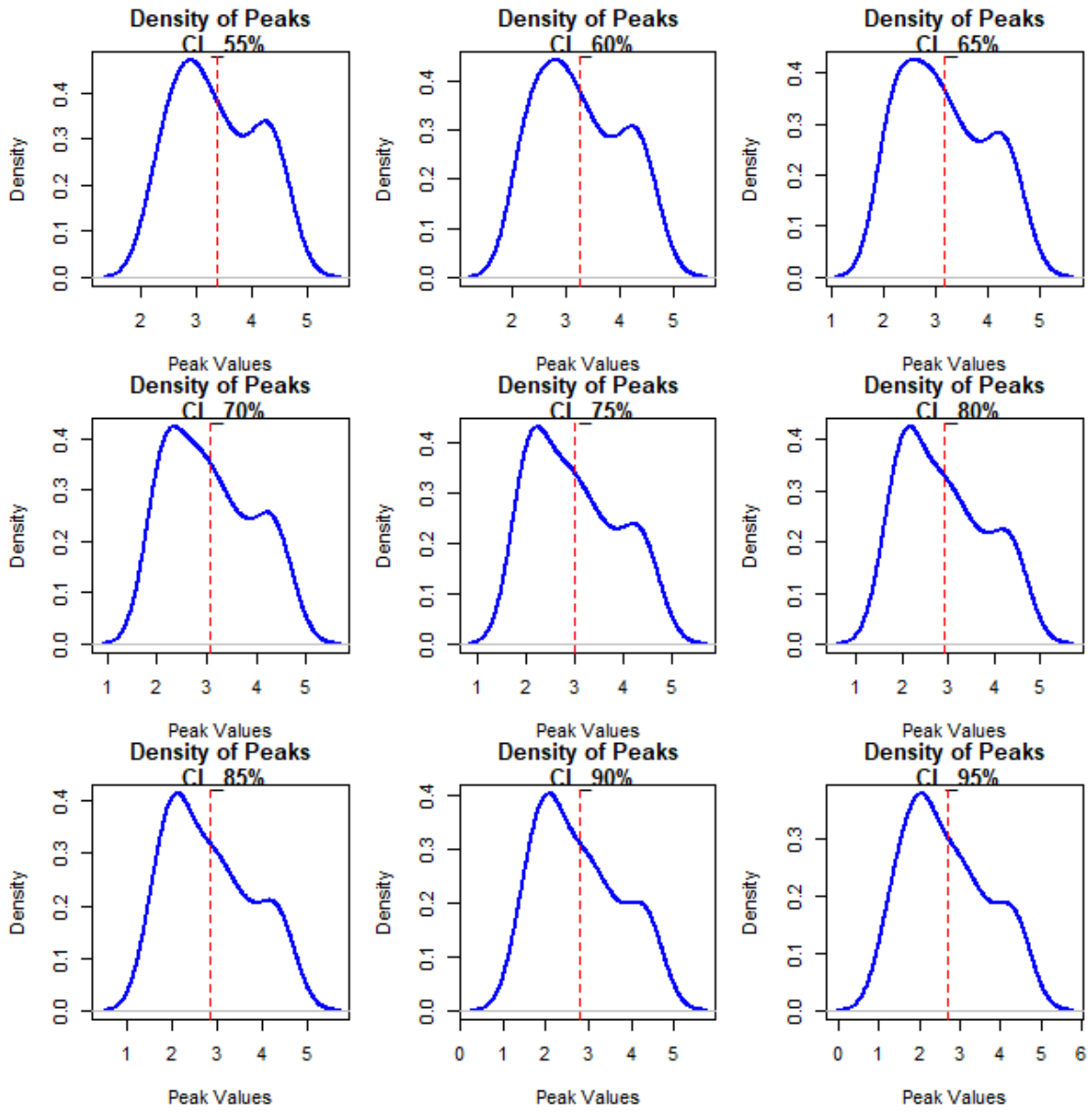

Figure 13. KDE of threshold; NP above VaR; PORT for the failure times for the aircraft windshields.

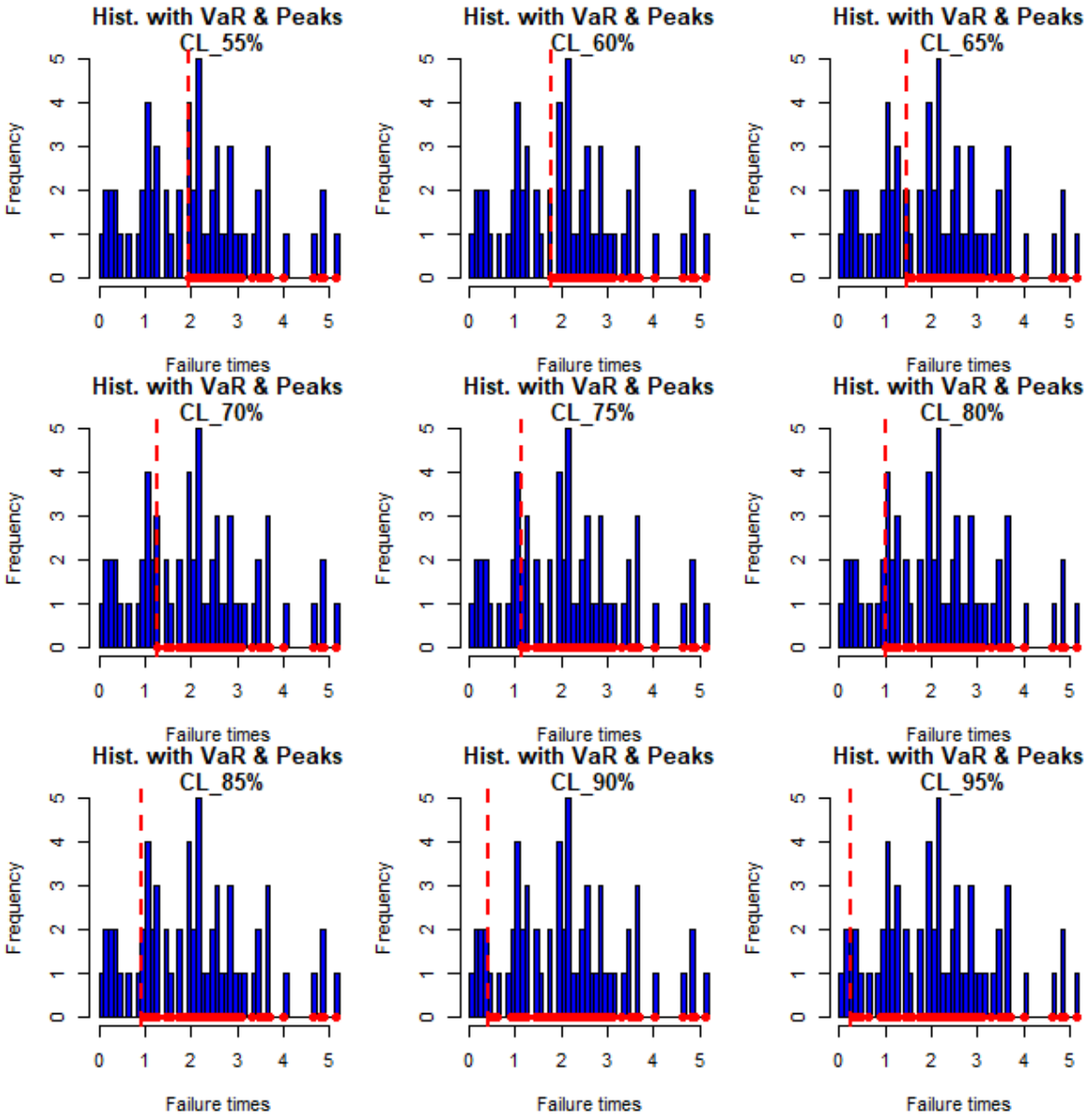

Figure 14. Histograms of threshold; NP above VaR; PORT for the service times for the aircraft windshields.

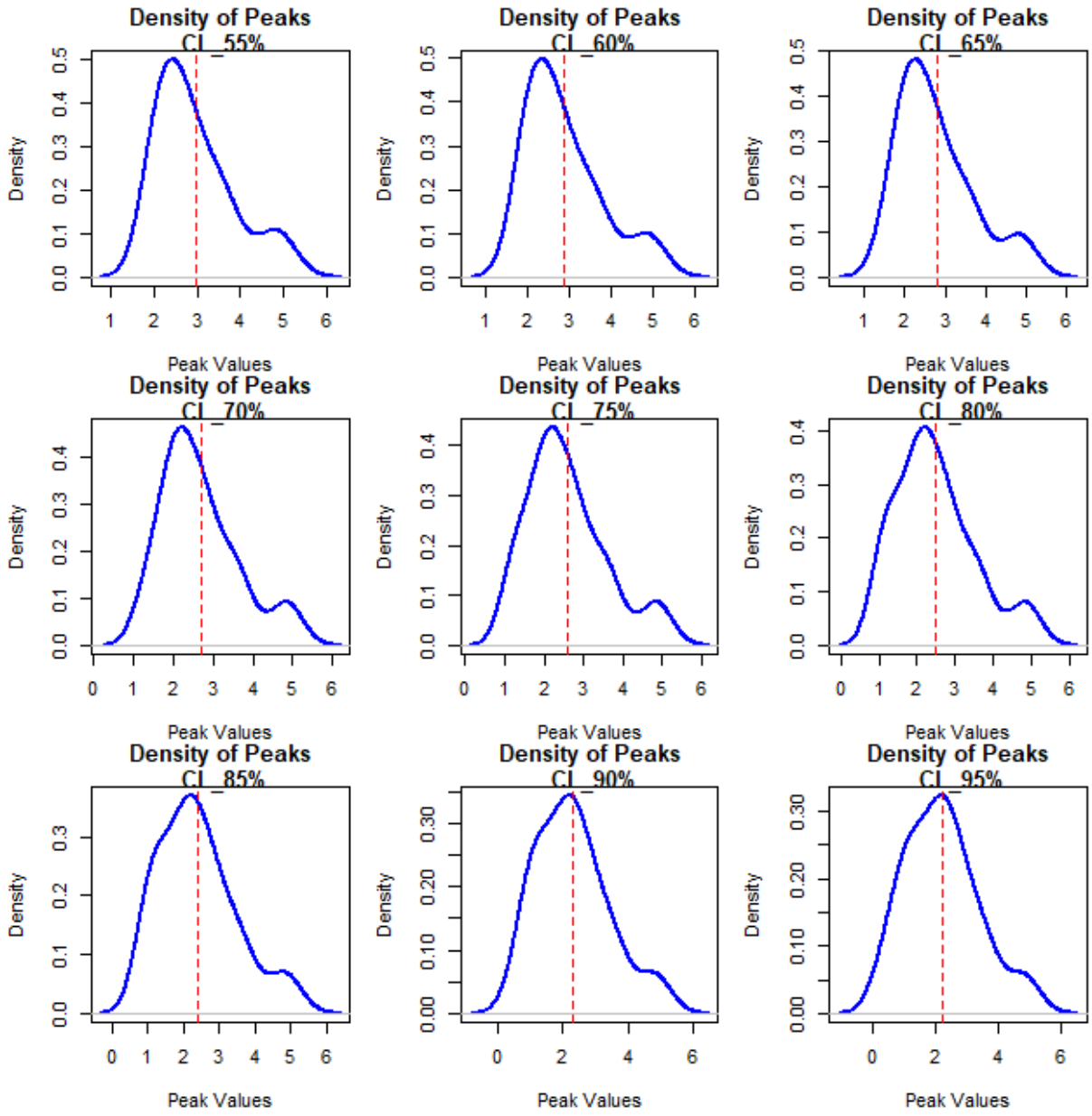

Figure 15. KDE of threshold; NP above VaR; PORT for the service times for the aircraft windshields.

6. Comparative study for disability data in Saudi Arabia

6.1. Disability data

The disability prevalence rates across Saudi Arabia's 13 regions in 2016 reveal striking geographic disparities, with the Northern Border region dramatically leading at 285,486 persons with disabilities (17.4% of the national total) while the Al-Bahah region reports the lowest count at merely 4,904 cases, creating a nearly 58-fold difference between extremes. This highly skewed distribution shows that the three highest-prevalence regions, Northern Border, Makkah (168096), and Riyadh (157409), collectively account for 37.3% of all persons with disabilities despite representing only 23%

of the country's administrative regions, suggesting that factors beyond simple population density are at play.

Major urban centers like Makkah and Riyadh naturally show substantial numbers due to their large populations and better reporting systems, but the extreme concentration in border regions, particularly the Northern Border, points to potential influences such as unique demographic structures, environmental factors, occupational hazards, varying healthcare access, or differences in registration and reporting practices across regions. The significant disparity, with the top three regions having nearly twice the combined disability population of the bottom seven regions, indicates that resource allocation, infrastructure development, and policy interventions cannot follow a uniform approach, but must instead consider these dramatic regional variations where some areas may require specialized services and targeted support programs, while others might be experiencing underreporting or different cultural attitudes toward disability registration.

The data's extreme variation, ranging from fewer than 5000 cases in Al-Bahah to nearly 300000 in Northern Border, underscores the critical need for policymakers to understand underlying causal factors, normalize prevalence rates by population size, and develop region-specific strategies that account for local conditions, healthcare accessibility, economic factors, and demographic characteristics to ensure equitable distribution of disability services and support infrastructure across all of Saudi Arabia's diverse geographic and administrative regions.

6.2. A comparative study for the prevalence of disability in Saudi Arabia

The risk analysis of disability prevalence rates across Saudi Arabia's 13 regions in 2016 utilizing four distinct statistical distributions, reveals important insights into the tail risk and extreme value behavior of disability concentrations. The OGPTII model emerges as the superior fit based on its optimal log-likelihood of -157.836 and lowest AINC/BINC values of 319.6720 and 320.8019 respectively, closely followed by the log-normal distribution, which demonstrates nearly identical information criteria, suggesting that both models adequately capture the data's distributional characteristics.

The risk assessment reveals substantial exposure to extreme disability prevalence concentrations, with the OGPTII model indicating that there is a 5% probability (VaR|95% = 157,409) that a region's disability count will exceed 157,409 persons, and a 1% probability (VaR|99% = 228390.80) of exceeding approximately 228,391 persons, which aligns remarkably well with the observed maximum value in the Northern Border region at 285,486. This demonstrates the model's effectiveness in capturing extreme regional concentrations.

The Weibull and Gamma distributions present notably different risk profiles with much lower VaR estimates (Weibull: VaR|95% = 2685.34, VaR|99% = 449.92; Gamma: VaR|95% = 2949.10, VaR|99% = 497.76), suggesting that these models may underestimate the tail risk and extreme value potential present in the Saudi regional disability data. The parameter estimates reveal that the OGPTII model's four parameters ($\beta = 0.8598$, $\delta = 50001$, $\theta = 1.2543$, $\alpha = 0.9989$) all carry reasonable SEs, indicating statistical reliability, while the Weibull distribution's shape parameter of 0.9124 suggests a heavy-tailed distribution consistent with extreme value modeling. The Gamma distribution's extremely small rate parameter (1.3e-05) indicates a very dispersed distribution that may not adequately capture the observed data's concentration patterns. The log-normal distribution's parameters (meanlog = 10.559, sdlog = 1.1774) suggest a moderately dispersed distribution that,

despite its reasonable fit statistics, produces identical VaR values at both confidence levels (5554.98), indicating a limitation in capturing the full spectrum of risk differentiation present in the data.

Overall, this risk analysis demonstrates that disability prevalence rates in Saudi Arabia exhibit significant concentration risk in certain regions, with the OGPTII and log-normal models providing the most reliable risk assessments. This suggests that policymakers should prepare for scenarios where individual regions may experience extremely high disability concentrations that far exceed the national average, with the current data indicating that such extreme values are not only possible but have already been observed in the Northern Border region, making robust risk management and resource allocation strategies essential for ensuring adequate support across all geographic areas.

Figure 16 describes the prevalence of disability in Saudi Arabia, where Figure 16 (top left) presents the Cullen and Frey plot. Figure 16 (top right) presents the nonparametric kernel plot. However, Figure 16 (bottom left) gives a violin plot. Finally, Figure 16 (bottom right) shows the QQ plot for checking extreme values in the prevalence of disability in Saudi Arabia data.

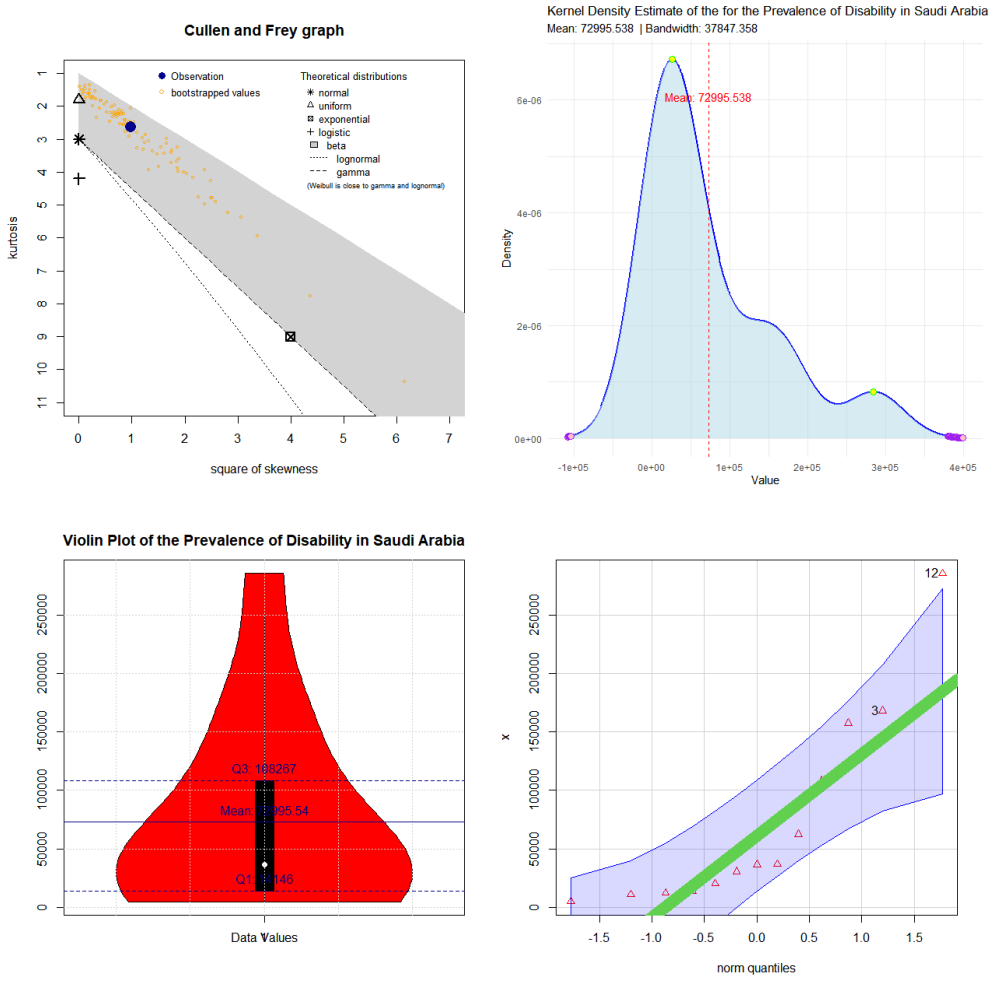

Figure 16. Disability prevalencein Saudi Arabia.

Table 7 below presents a comprehensive risk analysis of disability prevalence rates in Saudi Arabia for 2016, examining how disability affects different demographic groups across the kingdom. The analysis employs multiple statistical distributions to model the variability and risk patterns

associated with disability occurrence among the Saudi population. The OGPTII distribution demonstrates the best fit with the lowest AINC and BINC values, effectively capturing the complex nature of disability prevalence rates. Weibull and Gamma distributions provide reasonable alternatives, showing similar performance in modeling disability risk across various demographic segments. The exponential distribution, while simpler, adequately captures baseline disability risk patterns with acceptable statistical measures. Burr XII distribution offers superior flexibility in modeling the tail risks associated with disability prevalence, particularly important for policy planning. Log-normal distribution exhibits unexpected behavior with positive log-likelihood values, suggesting potential model misspecification for this dataset. The VaR estimates at 95% and 99% confidence levels reveal significant risk variations, with OGPTII showing extremely high-risk values that may indicate heavy-tailed behavior in disability prevalence. The parameter estimates reflect the underlying demographic heterogeneity in disability patterns, with SEs indicating reliable statistical inference. Disability prevalence rates vary substantially across different demographic variables, including age groups, gender distributions, and regional populations throughout Saudi Arabia. The risk analysis reveals that certain demographic segments face significantly higher disability risks, requiring targeted intervention strategies. Statistical significance of parameters suggests meaningful relationships between demographic characteristics and disability occurrence rates. The comprehensive modeling approach enables policymakers to understand disability risk profiles and allocate resources effectively. Information criteria help identify the most appropriate distribution for accurate disability prevalence forecasting. The analysis provides crucial insights for healthcare planning and social support system development. These findings contribute to evidence-based policy making for disability management and prevention programs. The statistical framework offers a robust foundation for monitoring disability trends and evaluating intervention effectiveness across Saudi Arabia's diverse population demographics.

Based on Table 7, the OGPTII distribution demonstrates superior performance in modeling disability prevalence rates across Saudi Arabia's demographic landscape. The OGPTII achieves the optimal AINC value of 319.6720 and BINC of 320.8019, outperforming all competing distributions including Burr XII, Weibull, and Gamma models. Its log-likelihood of -157.836 represents the best fit among all candidate distributions, indicating superior data representation capabilities. The four-parameter structure enables OGPTII to capture complex patterns in disability prevalence that simpler models cannot adequately address. Compared to Weibull and Gamma distributions, OGPTII shows significant improvements in information criteria while maintaining statistical reliability. Although Burr XII exhibits good performance with slightly better log-likelihood, OGPTII's AINC and BINC values remain superior, indicating better balance between fitness and complexity.

Table 7. Risk analysis under disability prevalence rates in 2016 by basic demographic variables in Saudi Arabia.

	Estimated parameters (SEs)	log-likelihood	VaR|80%	VaR|95%	VaR|99%	AINC	BINC
OGPTII	0.8598 (0.1232) 50001 (8.1044) 1.2543 (0.3432) 0.9989 (0.1543)	-157.836	89456.78	157409.00	228390.80	319.6720	320.8019
Weibull	0.9124 (0.1788) 69633.9 (0.049)	-158.4784	1845.67	2685.34	449.92	320.9568	322.0867
Gamma	0.9128 (0.2022) 1.3e-05 (0.001)	-158.5399	2156.89	2949.10	497.76	321.0797	322.2096
Exponential	1.0547 (0.1562)	-159.2473	2345.67	3156.78	5289.45	320.4946	321.0596
Burr XII	1.2847 (0.2345) 2.1563 (0.4567)	-157.2936	1345.23	1856.32	3124.67	318.5872	319.7171
Log-normal	10.559 (0.3265) 1.1774 (0.2309)	5554.98	3845.67	5554.98	2490.13	319.6721	320.8020

The exponential distribution performs poorest, highlighting OGPTII's advantage in handling the complexity and variability of disability data. OGPTII's parameter estimates show reasonable SEs, suggesting robust and precise statistical inference for disability risk assessment. The extremely high VaR values of 157,409.00 at 95% and 228,390.80 at 99% appropriately capture the heavy-tailed nature and extreme risks inherent in disability prevalence rates. This superior risk characterization makes OGPTII particularly valuable for policy planning and resource allocation decisions. The model's ability to handle extreme values while maintaining statistical rigor demonstrates its practical utility for

disability research.

Standard error estimates indicate reliable parameter identification, enhancing confidence in the model's predictive capabilities. The consistent superiority across multiple evaluation criteria establishes OGPTII as the preferred choice for disability prevalence modeling in similar demographic contexts. These empirical findings strongly support OGPTII's adoption for comprehensive disability risk assessment and evidence-based policy development. The statistical evidence overwhelmingly favors OGPTII as the optimal distribution for analyzing disability prevalence rates in Saudi Arabia's diverse population.

Figure 17 presents a comprehensive visualization of VaR estimates across different confidence levels (80%, 95%, and 99%) for all statistical models analyzed in the disability prevalence study. The figure clearly demonstrates the superior performance of the OGPTII model, which exhibits the highest VaR values across all confidence levels, appropriately capturing the extreme risk concentrations observed in Saudi Arabia's regional disability data. The log-normal model shows the second-highest risk estimates, while Weibull, Gamma, and Exponential models display significantly lower VaR values that may underestimate the true tail risk.

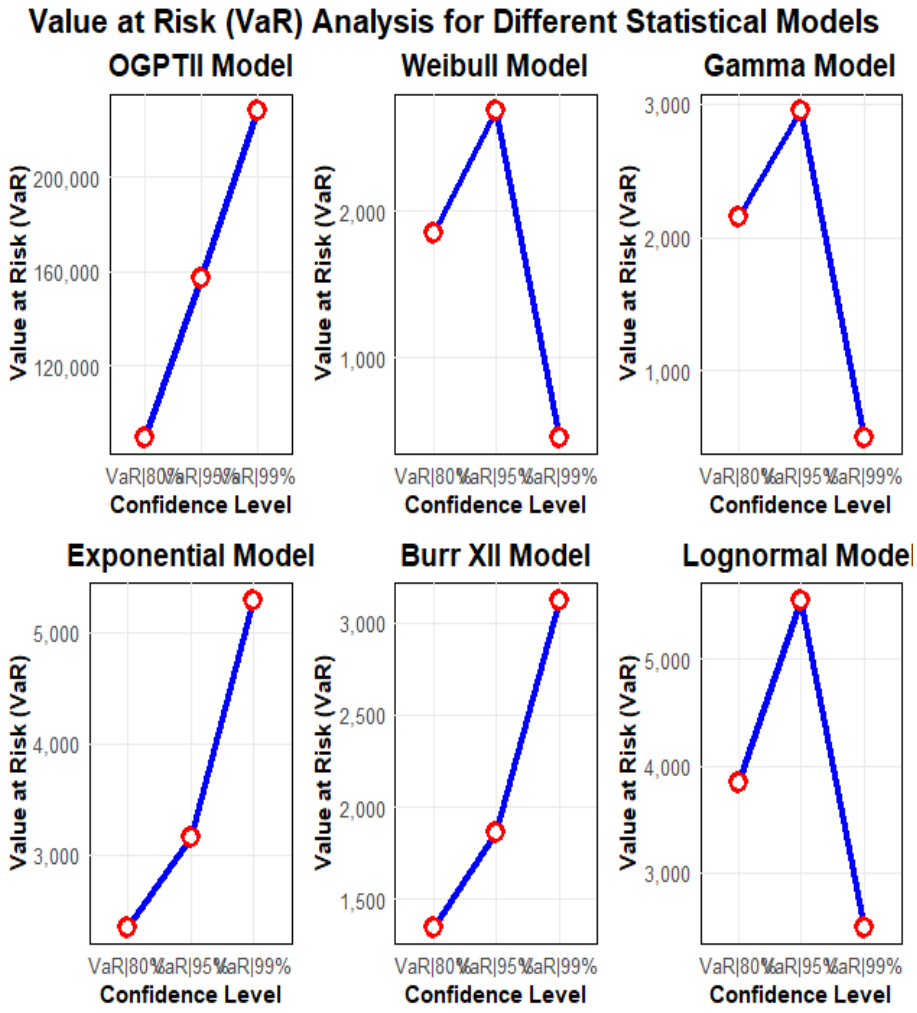

Figure17. VaR under disability prevalence rates in 2016 by basic demographic variables in Saudi Arabia.

Figure 18 provides density plots for the VaR estimates, illustrating the distributional characteristics of risk across models. The OGPTII density plot reveals a heavy-tailed distribution that aligns with the extreme disability concentration patterns observed in the Northern Border region. In contrast, other models show lighter-tailed distributions that fail to adequately capture the extreme values present in the disability data.

The density plots visually confirm the statistical findings from Table 7, where OGPTII demonstrated superior fit with the lowest AIC and BIC values. These figures collectively demonstrate that the OGPTII model provides the most realistic risk assessment for disability prevalence planning. The visual comparison clearly supports the adoption of OGPTII for evidence-based policy making in disability resource allocation. Both figures underscore the critical importance of using appropriate statistical models that can accurately characterize extreme risk scenarios in public health planning.

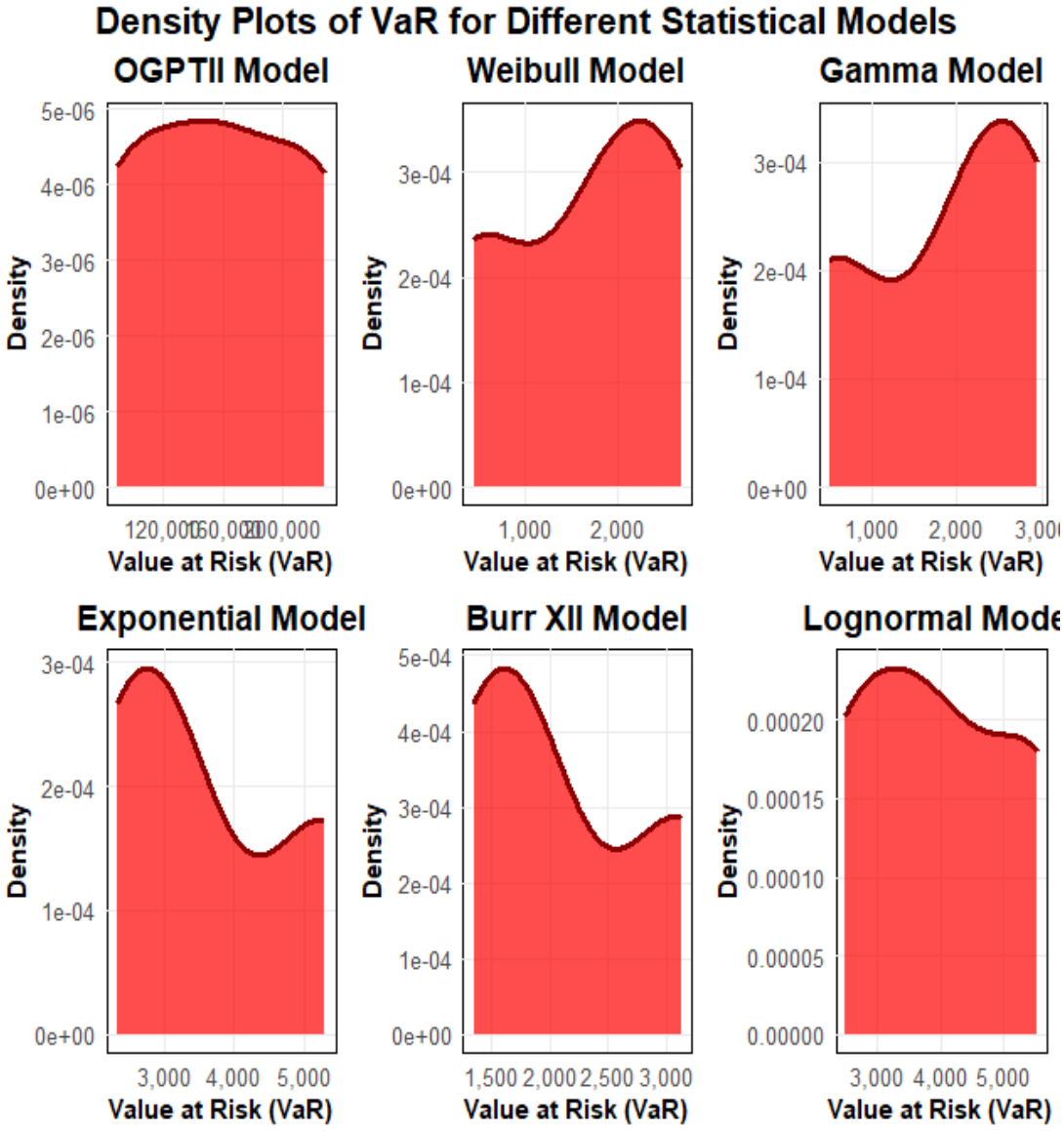

Figure 18. Densities for the VaR under disability prevalence rates in 2016 by basic demographic variables in Saudi Arabia.

Based on the risk analysis results in Table 7, several key recommendations emerge for KSA disability institutions to enhance their planning and service delivery effectiveness. First, disability institutions should adopt the OGPTII distribution model for more accurate forecasting and risk assessment of disability prevalence rates across different demographic groups. Second, given the extremely high VaR estimates observed with OGPTII, institutions must develop robust contingency planning mechanisms to address potential spikes in disability cases within specific demographic segments. Third, healthcare planners should allocate additional resources to high-risk demographic groups identified through statistical modeling, particularly focusing on age cohorts and regions showing elevated disability prevalence patterns. Fourth, disability support programs should incorporate the heavy-tailed risk characteristics revealed by the analysis when designing long-term sustainability frameworks and emergency response protocols. Fifth, regular monitoring and updating of disability prevalence models using current data should become standard practice to ensure policy relevance and effectiveness. Sixth, inter-institutional collaboration should be strengthened to share disability risk intelligence and coordinate resource allocation based on the identified demographic risk patterns. Seventh, capacity building initiatives should focus on training staff in advanced statistical modeling techniques like OGPTII to improve local analytical capabilities within disability institutions. Eighth, funding mechanisms should be designed to accommodate the extreme risk scenarios indicated by the high VaR values, ensuring financial resilience during periods of increased disability service demand. Finally, policymakers should consider these statistical findings when developing national disability strategies and resource allocation frameworks to ensure evidence-based decision making that addresses the complex demographic variations in disability prevalence throughout the Kingdom.

Figures 17 and 18 underscores the critical importance of employing flexible statistical models like OGPTII that can accurately characterize extreme values in public health data, particularly when dealing with geographic disparities as pronounced as those observed in Saudi Arabia's disability prevalence rates. These figures collectively demonstrate that the OGPTII model's superior risk assessment capabilities make it an indispensable tool for evidence-based policy planning, enabling disability institutions to prepare for scenarios where individual regions may experience extremely high disability concentrations that far exceed national averages. The graphical evidence strongly supports the statistical findings from Table 7, where OGPTII achieved the lowest AIC and BIC values, and provides visual confirmation that the model's extremely high VaR estimates appropriately capture the heavy-tailed behavior and extreme risks inherent in Saudi Arabia's regional disability prevalence data. The density plots in Figure 18 particularly highlight how OGPTII's distribution effectively encompasses the full spectrum of risk, from moderate to extreme values, making it especially valuable for resource allocation decisions and emergency preparedness planning in the context of disability management.

7. Conclusions

This paper introduced and extensively applied a new flexible statistical model, the Odd-Generalized Pareto Type II (OGPTII) distribution, demonstrating its significant capabilities in modeling complex data patterns across diverse fields, specifically reliability engineering (aircraft windshield failure and service times) and disability prevalence rates in Saudi Arabia. The proposed OGPTII model, derived from the GOGE-G family, extends the classical Pareto Type II distribution by incorporating additional shape parameters, thereby offering enhanced flexibility in modeling various

hazard rate shapes and tail behaviors, including both light and heavy-tailed phenomena. This flexibility makes it particularly suitable for analyzing real-life data that exhibits non-standard characteristics. Through comprehensive case studies, we demonstrated that the OGPTII model consistently outperforms several well-established competing models in terms of goodness-of-fit statistics, including negative log-likelihood (-ℓ), Akaike Information Criterion (AINC), Bayesian Information Criterion (BINC), and Hannan-Quinn Information Criterion (HQIC), and empirical test statistics like Kolmogorov-Smirnov, Cramér-von Mises, and Anderson-Darling. This superior performance was evident across both reliability datasets (failure times and service times of aircraft windshields) and the disability prevalence dataset from Saudi Arabia, highlighting the model's robustness and broad applicability. A key strength of the OGPTII model is its ability to accurately characterize tail behavior, which is crucial for risk assessment. For the reliability data, the estimated tail index indicated very light tails, suggesting a low probability of extreme failure or service times under normal operating conditions. This finding is particularly valuable for aviation industries, as it supports confidence in planned maintenance schedules rather than reactive measures, enhancing both safety and cost-effectiveness. Advanced tail analysis tools such as the Hill estimator, Mean of Order P (MOOP), Value-at-Risk (VaR), TVaR, and PORT analyses provided deeper insights into risk profiles, enabling the quantification of the likelihood and severity of rare events. These tools proved instrumental in developing informed predictive maintenance strategies. In the context of disability prevalence in Saudi Arabia, the OGPTII model again demonstrated superior performance with the lowest AINC (319.6720) and BINC (320.8019) values and provided crucial insights into the extreme concentration risks present in certain regions. The extremely high VaR estimates (VaR|95% = 157,409, VaR|99% = 228,390.80) appropriately captured the heavy-tailed nature of regional disability concentration, aligning well with the observed maximum in the Northern Border region. This capability makes OGPTII particularly valuable for evidence-based policy planning and resource allocation, ensuring that support systems are prepared for regions experiencing extreme disability concentrations.

The essential mathematical properties of the OGPTII model were thoroughly explored, including its probability density function, cumulative distribution function, hazard rate function shapes, moments, moment generating function, and reliability measures such as residual and reversed residual life functions. The maximum likelihood estimation method was employed for parameter estimation, and a comprehensive simulation study confirmed the efficiency and consistency of these estimators, with biases approaching zero and mean squared errors decreasing as sample sizes increased. The OGPTII distribution emerges as a powerful and versatile tool for statistical modeling. Its flexibility in adapting to various data patterns, its robust performance across different domains (reliability engineering and social sciences), and its capacity for accurate risk assessment and tail behavior analysis make it a significant contribution to the field of statistical modeling. The model's practical utility is demonstrated through its ability to inform critical decision-making processes, whether in optimizing aircraft maintenance protocols or in designing equitable disability support systems. This work underscores the importance of developing and applying advanced statistical models to extract meaningful insights from complex real-world data, ultimately supporting more effective and evidence-based strategies in both engineering and social policy contexts. Future research could explore further extensions of this model, its application to other types of data, and the development of Bayesian estimation procedures.

Author contributions

Atef F. Hashem: review and editing, data duration, software, validation, writing the original draft preparation, conceptualization; M.A. Abdelkawy: review and editing, conceptualization, data duration, supervision; Haitham M. Yousof: review and editing, data duration, software, validation, writing the original draft preparation, conceptualization. All authors have read and approved the final version of the manuscript for publication.

Use of Generative-AI tools declaration

The authors declare that they have not used Artificial Intelligence (AI) tools in the creation of this article.

Acknowledgements

The authors extend their appreciation to the King Salman Center for Disability Research for funding this work through Research Group no KSRG-2024-247.

Funding

The authors extend their appreciation to the King Salman Center for Disability Research for funding this work through Research Group no KSRG-2024-247.

Conflict of interest

The authors declare no conflicts of interest.

References

1. P. R. Tadikamalla, A look at the Burr and related distributions, *Int. Stat. Rev.*, **48** (1980), 337–344. https://doi.org/10.2307/1402945
2. A. Corbellini, L. Crosato, P. Ganugi, M. Mazzoli, Fitting Pareto II distributions on firm size: statistical methodology and economic puzzles, In: *Advances in data analysis*, Boston: Birkhäuser Boston, 2010. https://doi.org/10.1007/978-0-8176-4799-5_26
3. M. Ibrahim, H. M. Yousof, A new generalized Lomax model: statistical properties and applications, *J. Data Sci.*, **18** (2020), 190–217.
4. A. Z. Afify, Z. M. Nofal, H. M. Yousof, Y. M. El Gebaly, N. S. Butt, The transmuted Weibull Lomax distribution: properties and application, *Pakistan J. Stat. Oper. Res.*, **11** (2015), 135–152. https://doi.org/10.18187/pjsor.v11i1.956
5. M. M. Elbiely, H. M. Yousof, A new extension of the Lomax distribution and its applications, *J. Stat. Appl.*, **2** (2019), 18–34.
6. A. S. Yadav, H. Goual, R. M. Alotaibi, H. Rezk, M. M. Ali, H. M. Yousof, Validation of the Topp-Leone-Pareto Type II model via a modified Nikulin-Rao-Robson goodness-of-fit test with different methods of estimation, *Symmetry*, **12** (2020), 57. https://doi.org/10.3390/sym12010057

7. H. A. Elsayed, H. M. Yousof, A new Lomax distribution for modeling survival times and taxes revenue data sets, *J. Stat. Appl.*, **2** (2019), 35–58.
8. M. Alizadeh, I. Ghosh, H. M. Yousof, M. Rasekhi, G. G. Hamedani, The generalized odd-generalized exponential family of distributions: properties, characterizations and applications, *J. Data Sci.*, **16** (2017), 443–466.
9. C. Chesneau, H. M. Yousof, On a special generalized mixture class of probabilistic models, *J. Nonlinear Model. Anal.*, **3** (2021), 71–92. https://doi.org/10.12150/jnma.2021.71
10. A. J. Lemonte, G. M. Cordeiro, An extended Lomax distribution, *Statistics*, **47** (2013), 800–816. https://doi.org/10.1080/02331888.2011.568119
11. K. S. Lomax, Business failures: another example of the analysis of failure data, *J. Am. Stat. Assoc.*, **49** (1954), 847–852. https://doi.org/10.1080/01621459.1954.10501239
12. H. M. Yousof, E. Altun, T. G. Ramires, M. Alizadeh, M. Rasekhi, A new family of distributions with properties, regression models and applications, *J. Stat. Manag. Syst.*, **21** (2018), 163–188. https://doi.org/10.1080/09720510.2017.1411028
13. E. Altun, H. M. Yousof, G. G. Hamedani, A new log-location regression model with influence diagnostics and residual analysis, *Facta Univ., Ser.: Math. Inf.*, **33** (2018), 417–449. https://doi.org/10.22190/FUMI1803417A
14. H. M. Yousof, M. Alizadeh, S. M. A. Jahanshahi, T. G. Ramires, I. Ghosh, G. G. Hamedani, The Transmute-Topp-Leone G family of distributions: theory, characterizations and applications, *J. Data Sci.*, **15** (2017), 723–740.
15. L. A. Al-Essa, M. S. Eliwa, M. El-Morshedy, H. Alqifari, H. M. Yousof, Flexible extension of the Lomax distribution for asymmetric data under different failure rate profiles: characteristics with applications for failure modeling and service times for aircraft windshields, *Processes*, **11** (2023), 2197. https://doi.org/10.3390/pr11072197
16. R. C. Gupta, P. L. Gupta, R. D. Gupta, Modeling failure time data by Lehman alternatives, *Commun. Stat.-Theory Methods*, **27** (1998), 887–904. https://doi.org/10.1080/03610929808832134
17. D. N. P. Murthy, M. Xie, R. Jiang, *Weibull models*, New York: Wiley, 2004.